UNIVERSIDAD CARLOS III

Bachelor's Degree in Aerospace Engineering
2016/2017

Bachelor Thesis

Analysis of Spacecraft Charging in several space environments

---

Betsabé Moreno Campos

Director
Antonio Sanchez Torres
September 2017

To my grandmother Lola,
the strongest person I have ever met

Abstract

Since the first days of space era, the effects of the space environment in spacecraft were considered a critical issue. Spacecraft charging is one of the most damaging effects of space environment. This work presents this phenomenon, focusing on surface spacecraft charging. This is studied through the Equipot tool that allows to study surface charging in spacecraft at Earth's environment. It has been performed a sensitive analysis using this code and the results were compared with similar analysis presented in 1989. Considering the expansion of the space technology along the Solar system, it has been considered to broaden the study of this phenomenon to other planets. Therefore, it is also presented in this bachelor thesis the implementation of a Matlab code for the study of spacecraft charging at Jupiter and Saturn's magnetospheres.

Acknowledgements

I would like to thank professor Antonio Sanchez Torres whose dedication, help and patience through the last year have been essential in the development and writing of this work.

I have been fortunate to receive the supports of all my friends. In special, I am particularly grateful for being part of the Noble and Discreet Order of the Silver Wing. Thank you for these last 5 years of adventures.

This bachelor thesis would not be possible without my family. I really know the sacrifice that they had made to make possible for me to study at the university. I specially want to thank my parents for encouraging me to reach all I have reached and to go further. I would also like to mention my siblings for their daily support.

Finally, I need to mention Alejandro, my partner in this long journey. It is thanks to him that I have the enough strength to arrive at this point. He gave me all his support and patience even when the difficult times arrived. Thank you for being my light when everything else was dark.

The sky was never the limit,

Betsabé

Contents

List of Figures

List of Tables

Chapter 1

Introduction

In April 2010, ground controllers lost contact with the Galaxy 15 telecommunications satellite. It begun to wander without control with no possibility of executing station keeping maneuvers. This became a threat of getting in the way of other spacecraft and potentially affecting their transmissions. This situation lasted for months. Fortunately, the control of this satellite could be restored. Later studies revealed that this incident was due to spacecraft charging. [1]

There is a strong tendency in people to think about Space as an enormous empty void between stars, planets, asteroids, etc. Nothing further from reality. Within our Solar System, interstellar space is filled with plasma expelled by solar wind. Plasma is one of the four fundamentals state of the matter. It is the most common phase in the universe. Spacecraft near Earth, spacecraft operates within plasmasphere, the ionosphere, and polar wind. Plasmasphere (or inner magnetosphere) is a region of the Earth's magnetosphere consisting of low energy plasma. Ionosphere is the upper region of the Earth's atmosphere and forms the inner edge of the magnetosphere of our planet. Polar wind is an outflow of plasma from the polar regions of the Earth's magnetosphere. It is caused by the interaction between the Earht's atmosphere and solar wind. When running at these conditions, charged particle impacts constantly the surfaces of spacecrafts, producing a charging process in them.

This charging process is known as spacecraft charging. It could be on the surface (absolute or differential charging), if the process only occurs at the external surfaces of the spacecraft; or deep internal charging, when the charged particles go through the spacecraft and affects internal elements.

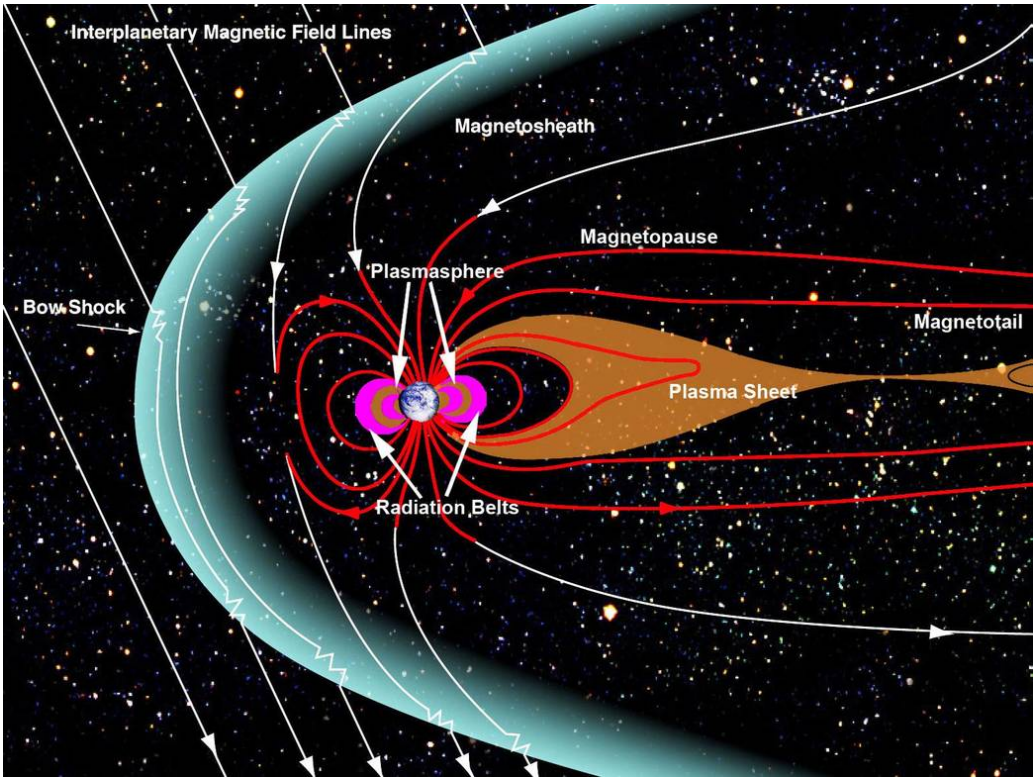

Figure 1.1: Earth's Magnetosphere [2]

However, spacecraft charging is not always produced as an effect of the environment where the body is in. Electric propulsion that has been developed recently is another source of this phenomenon. The plume of space plasma thruster may interact with the surfaces producing a spacecraft charging issue.

1.1 Spacecraft Charging: Why do we should study this phenomenon?

Spacecraft charging is not harmful by itself, it is the discharging that produces the hazard. Dissimilar materials, movement through space, different radiation affecting different spots,etc. There are a lot of potential causes that produces charging differently along the surface of the spacecraft. If the difference between potential is very high, it will lead to Electrostatic discharge (ESD) that produce numerous damages in the structure.

The damages may provoke malfunction of the systems. As the case commented previously, there are many possibilities that spacecraft can suffer the effects of spacecraft charging. The ESD may produce a displacement of the satellite or modify its attitude, moving it to a different trajectory where it is possible to interfere other close spacecraft; a cutoff in the communications ground-space that prevents to modify any aspect produced in the malfunction of this satellite; and other possible events. Spacecraft charging is also dangerous because it could affect the measurement devices of the satellite. That means, it is possible that the high concentration of charged particles will produce misunderstand when doing measurements. It will be collected erroneous data that could be fatal depending on the mission of the sensors.

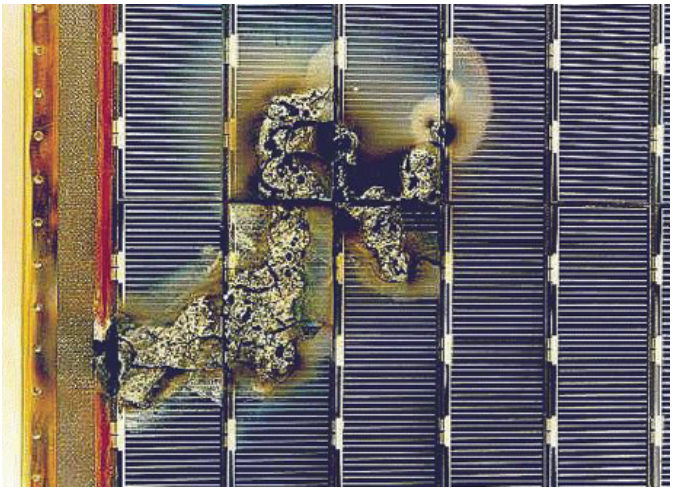

Figure 1.2: ESA EURECA satellite solar array sustained arc damage. [1]

In 1999, there was published a paper about the impact of the space environment on space systems [3]. It introduced a study about the different anomalies founded on space system due to different effects of the space environment. 326 Space environment impacts form were completed for this study. These impacts were divided into groups by anomaly diagnosis. The ESD anomalies group contains 162 forms, being the group with the major number of forms. This study shows the importance of studying space weather and spacecraft charging for the industry. In figure 1.3 it is possible to see a graphical representation of this research, where, as commented previously, the ESD group is the most noticeable one.

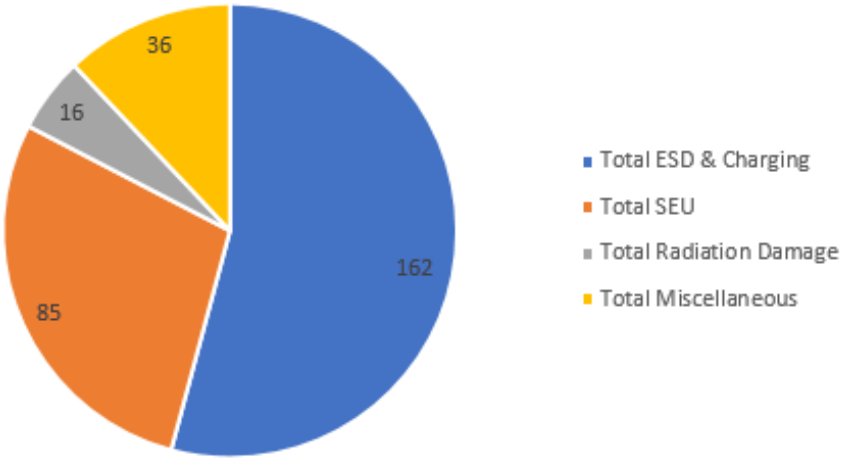

Figure 1.3: Anomalies founded on space system. Graphical representation

In 1995, it was published the NASA reference Publication 1375 [4] which verse about failures and anomalies attributes to Spacecraft charging. In this paper, it is possible to found a little compilation of cases where spacecraft charging produces anomalies that affected the mission. Not all missions detailed there were catastrophic or failure ones, but it is important to remark (as it is done in the paper) that even the small anomaly is important to be considered because a series of these kind of irregularities in the running of a spacecraft increase the chance for more significant

problems. In addition to the fact that even a little malfunction in the spacecraft led to an important cost for the mission.

Vehicle	Date	Diagnosis
DSCS II	1973	Loss of Mission
Voyager 1	1979	Anomaly at a Jupiter's Orbit
SCATHA	1982	Anomaly
GOES 4	1982	Loss of Mission
AUSSAT-A1, -A2, -A3	1986-1990	Anomaly
FLTSATCOM 6071	1987	Anomaly
GOES 7	1987-1989	System Failure
Feng Yun	1988	Loss of Mission
MOP-1, -2	1989-1994	Anomaly
BS-3A	1990	Anomaly
GMS-4	1991	Anomaly
MARECS A	1991	Loss of Mission
Anik E1	1991	Loss of Mission
Anik E2	1991	Anomaly
Intelsat 511	1995	Anomaly
SAMPEX	1992-2001	Anomaly
Intelsat K	1994	Anomaly
DMSP F13	1995	Anomaly
Telstar 401	1997	Loss of Mission
TSS-1R	1996	System Failure
TDRS F-1	1986-1988	Anomaly
TDRS F-3, F-4	1989-1998	Anomaly
INSAT 2D	1997	Loss of Mission
Tempo-2	1997	Loss of Mission
PAS-6	1997	Loss of Mission
Feng Yun 1C	1999	Anomaly
Ladsat 7	1999-2003	Anomaly
ADEOS-II	2003	Anomaly
TC-1,2	2004	Anomaly
Galaxy 15	2010	Anomaly
Echostar 129	2011	Anomaly
Suomi NPP	2011-2014	Anomaly

Table 1.1: Anomalies and Failures Atributed to Spacecraft Charging [5]

In 2014, it was presented an updated relation of missions affected by spacecraft charging at Spacecraft Anomalies and Future Workshop [5]. Table 1.1 shows these missions and whether it was a simple anomaly, a failure of one system or a mission loss. It is possible to appreciate the reduction in the number of incidents related with spacecraft charging in the last years. One important reason for this is the development of mitigation techniques used to alleviate the charging effects.

However, spacecraft charging is not always a damaging effect. Nowadays, there are studies about how can we use this phenomenon in our benefit in development, like deorbiting space debris or asteroid deflection. Bombaerdelli et al. [6] proposed an electrostactic tractor for deflection of near Earth's orbit. It exploits the interaction between a spacecraft and an asteroid, considering this interaction as the sum of the gravitational and electrostatic forces. The efficacy of this concept depends on the amount of this electrostatic forces, therefore on the amount of charge possible to maintain on spacecraft and asteroid. By other side, Schaub et al. [7] proposed another similar electrostatic tractor focused on deorbiting space debris by transferring the charge through ion or electron beam.

1.2 International Space Station: Issues related with spacecraft charging

The International Space Station (ISS) is the largest manned spacecraft orbiting the Earth. It is submerged in the space plasma, therefore due to its size and its movement around the Earth, the charging of this body is a critical issue. In addition, the presence of human beings adds a factor in the possible effects of this process.

The stored charge results in a floating potential of few tens of volts relative to the surrounding plasma. In addition, there is a positive charging caused by the motion of the ISS in the Earth's magnetic field (also known as Motional Electric Field).Besides the already mentioned effects of spacecraft charging that are fully applicable to ISS, the human factor takes a primordial role in this case. The ESD produced for a potential difference is fatal to safety of the crew.

The result of a spacecraft moving across a magnetic field is an electric field. The body will see a motional electric field imposed on it given by $\vec{E} = \vec{V_0} x \vec{B}$ [8]. This motional electric field produces that the differential between a spacecraft and the surrounding plasma varies with position on the body. At Earth's magnetosphere, this contribution is small unless the body has large size. Nowadays, the only spacecraft where this contribution can be consistent is ISS, where the potential difference from on end to the other may be of 26 V. By other side, if the spacecraft is placed at environment with a greater magnetic field, it is possible that this field affects smaller bodies. It is the case for mission near Jupiter's magnetosphere.

In 1987, Hall et al. [9] studied the effect of the spacecraft charging of an astronaut during an Extravehicula Activity (EVA). During this experiment, the astronaut was shown to charge above -4000 V. It was led to a potential difference of 840 V between astronaut and shuttle. Throughout laboratory testing, it is shown that many types of discharges could occur, leading to suit material and EVA equipment damage. In 2001, the risk of discharges through EVA crew was elevated to one of the top ISS program risks.

At ISS, there are several elements that increases the ESD hazard: spacecraft metallic structure, high potential solar power arrays, artificial plasma produced by ISS, EVA suits and tools, etc. In addition, while EVA crewperson is not bonded to structure. Fig 1.4 shows the multiple sensible point where the ESD can impact when performing an EVA.

This potential difference is usually produce by negative charging. This hazard problem was

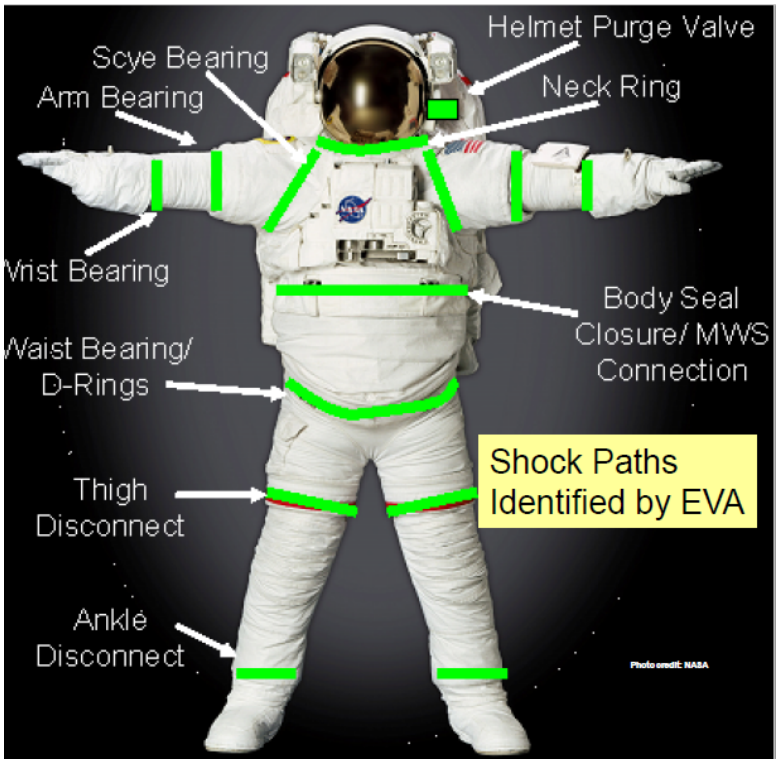

Figure 1.4: Crew sensible points where ESD can occur [10]

solved by introducing Plasma Contactor Unit (PCU). This tool forces collected electron into the environment in form of charged particle creating a slow neutral bath around ISS. The station has redundant PCUs in case of failure. This unit is more effective thanks to the possibility of monitoring the space environment through the Plasma Interaction Model (PIM) and the Floating Potential Measurement Unit (FPMU). The second system was developed by Utah State University's Space Dynamics Laboratory (USU-SDL) to study surface charging of the International Space Station.

PIM uses plasma density and temperature derived from from International Reference Ionosphere (IRI) model to predict the ISS charging levels. The IRI model is an empirical model which provides user with global and temporal variations of electron density and temperature, ion temperature and composition, ion drift, and total electron content.

Regarding positive electric charging, the motional electric field is the main reason of this hazard. It is also amplified in concentrated field near Earth's poles. Paradoxically, the PCU (that mitigates the effect of negative charging) increases this positive threat. There have been implemented several techniques to mitigate this effect. They will be seen in future sections in detail.Nowadays, thanks to the mitigation techniques, the risks are alleviated to a level that is orders of magnitude safer that prior operations.

1.3 Socioeconomic Impact of spacecraft charging

In 2016, it was launched 216 satellites. Space industry is a growing sector. Following the last State of Satellite Industry Report from the Satellite Industry Association (SIA) [11], the number of operational satellites has grown 47 % in five years (From 994 in 2012 up to near 1500 in 2016). In the last year, the revenues obtained by the Space Industry were 260.5 billion dollars; near the half of which came from Satellite Services.

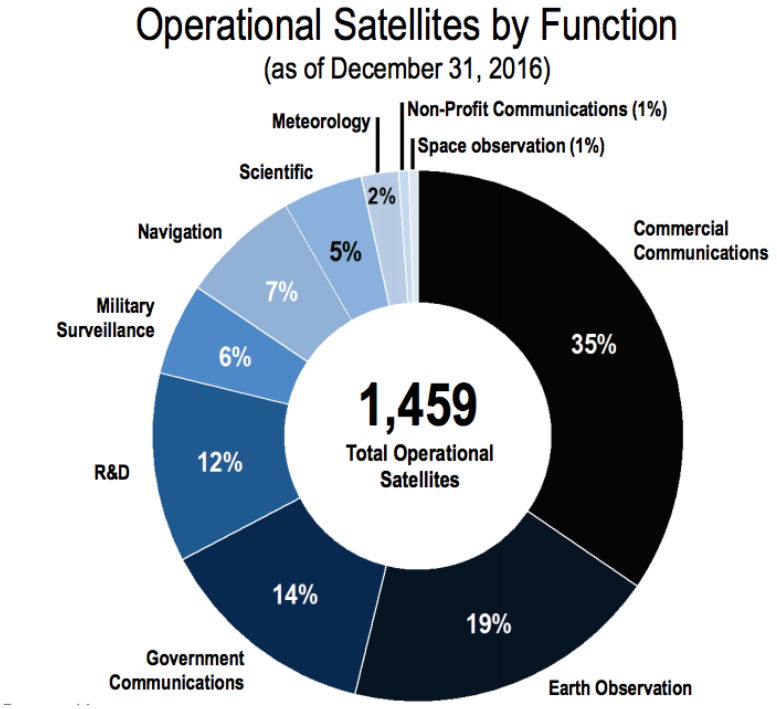

Figure 1.5: Operational Satellites by function [11]

The Satellite Industry is a main player inside the Space economy. The mission loss of one of the mentioned satellites would produce important losses to the industry. In January 1994, Anik-E2 communication satellite begun to spin out of control and it was not possible to activate the backup system. It was necessary to switch the services to other satellites, to realign ground equipment, to change frequencies, etc. The satellite was inoperative until August 1994, when the Telsat engineers restored it to service. Although the mission had not a fatal fail and it was possible to fix it, it was lost about $228 million assets and revenues of an estimated $3 billion.

Spacecraft charging is one of the effects produced by the environment interactions with the spacecraft and by the space weather. As mentioned before, the losses produced by a failure in-mission are highly enough to take care about this. This kind of failure has low probabilities to justify the insurance premiums. Therefore, it is crucial to study these effects and try to prevent them.

Additionally, exploration missions of sun, planets and their moons do require a deep study in space charging issues. NASA's Galileo mission completed several flybys over Jupiter, passing through intense radiation belts. The radiation dose in Galileo spacecraft was much higher than it was previously considered. With a deep study of environment, spacecraft charging effects and

using both passive and active mitigation techniques , risks of failures in navigation systems or scientific instruments will be reduced, avoiding to lose great amount of money

The European Space Agency (ESA) has a specific program designated to the analysis of space weather. This is called Space Situational Awareness (SSA) program [12]. Following the Space Weather (SWE) Study Results published by PwC [13] in November 2016, the benefit to cost ratio for space weather is 6.25 In figure 1.6 it is possible to see a summary of the cost of this analysis. It is fascinating to notice that the benefits of using this program are raised to near $3 million.

Summary of SWE Cost Benefit Analysis*

Reported as NPVs over 2016-2032

Cost/Benefit	'Do nothing scenario'	'Do ESA scenario'	Value added of ESA services
User domain benefits			
Satellite operations	- €293 M	- €267 M	€26 M
Launch operations (lower bound**)	- €0.3 M	- €0.1 M	€0.2 M
Resource exploitation	- €327 M	- €135 M	€192 M
Power grids operations	- €5,771 M	- €4,546 M	€1,225 M
Aviation	- €3,312 M	- €3,066 M	€246 M
Logistic/Road transport (lower bound**)	- €3,432 M	- €2,888 M	€544 M
Investment benefits GDP impact***	None	€904 M	€904M
Total benefits	**- €13,135 M**	**- € 9,998 M**	**- € 3,137 M**
ESA SWE Programme Costs (CAPEX + OPEX)	**None**	**- €502 M**	**- €502 M**
TOTAL	**- €13,135 M**	**- €10,500 M**	**€ 2,635 M**

Benefit to Cost ratio for SWE is 6.25

Figure 1.6: Summary of SWE Cost-Benefit Analysis [13]

On the other hand, the impact of the spacecraft charging is not only monetary. In a fatal failure of the satellite systems due to an ESD, the body can loss communication with ground (as it was happened with the previous examples). If this body begins to wander without control and no possibility of contact; it is highly probable that a collision with other spacecraft occurs. This would lead firstly in a legal issue regarding space debris and secondly, in an international conflict if affects other satellite from different country.

1.4 Objectives and procedure

The preceding sections have highlighted the importance of studying the space weather effects in spacecraft: structural damages, human threat, economic losses, etc. This bachelor thesis will focus in spacecraft charging, one of the most important hazard related with space weather and environmental interactions. As it is an extensive topic to talk about, it will concentrate in the analysis of this phenomenon through a simple charging code that allows to determine its magnitude for different environments and materials. This tool is called EQUIPOT. Afterwards, it will be presented an

approach of spacecraft charging in Jupiter and Saturn. Lastly, it will be presented the techniques used in order to mitigate the effects produced by the spacecraft charging.

In Section 2, the theoretical concepts of Spacecraft charging will be presented; as well as the state of art and its legal framework. Within this section, it will also explain a brief summary of different mitigation techniques. In Section 3, the tool EQUIPOT is presented. Consequently, a sensitive analysis is presented in the form of comparison with the already analysis done by Wrenn and Sims in 1989. [14]. This code only performs analysis in Earth's environments. Considering that the implementation of other planet's environment is in process to be included in EQUIPOT, it would be interesting to study this topic in Jupiter and Saturn's magnetospheres. Section 4 will deal with this issue. Finally, conclusions and further work is considered in section 5.

Section 2 will be about the physics that are applied in the study of Spacecraft Charging. It will be focus in the concepts that are applied at Earth's orbits. After that, a summary of studies already performed and the state of studies about this topic nowadays will be stated. Different tools for the study of spacecraft charging will be presented, together with a summary of mitigation techniques used to alleviate the effects of this phenomenon and a brief list of important standard documents.

Section 3 will present the tool EQUIPOT. As it will be explained later, EQUIPOT is used for preliminary studies about surface spacecraft charging. It will be shown a comprehensive analysis of this code, comparing it with a similar sensitive analysis performed in 1989.

Regarding section 4, the study of spacecraft charging will be address at Jupiter and Saturn environments. The idea is to take the code used in EQUIPOT and modify it to make possible the application of it to these magnetospheres.

1.5 Time Planning

This bachelor thesis has been developed since January 2017. In fig 1.7 plan it is possible to see the schedule followed. Four principal phases can be differentiated in time as it is shown in the figure.

The initial phase was dedicated to documentation. This phase includes the time dedicated exclusively to research and study of the theory needed to develop the thesis. This phase lasts from the beginning up to March. After that, a second documentation phase was performed parallel to other phases of the project.

Once the basis of the thesis has been understood and prepared, it has been performed the analysis using EQUIPOT. This phase takes from March to the end of April. In this phase, it is considered the time needed to learn to use EQUIPOT and perform the sensitive analysis.

After doing these two preliminary phases, it was considered that it would interesting to implement a code analyzing the magnetospheres of Jupiter and Saturn. This phase begins in May, when it is considered to introduce the values of Jupiter's magnetosphere in EQUIPOT tool. Finally, this idea was rejected and it started the implement of the modified code in Matlab. This phase finished at the end of July.

As a final period, from August the writing of the thesis became the principal task.

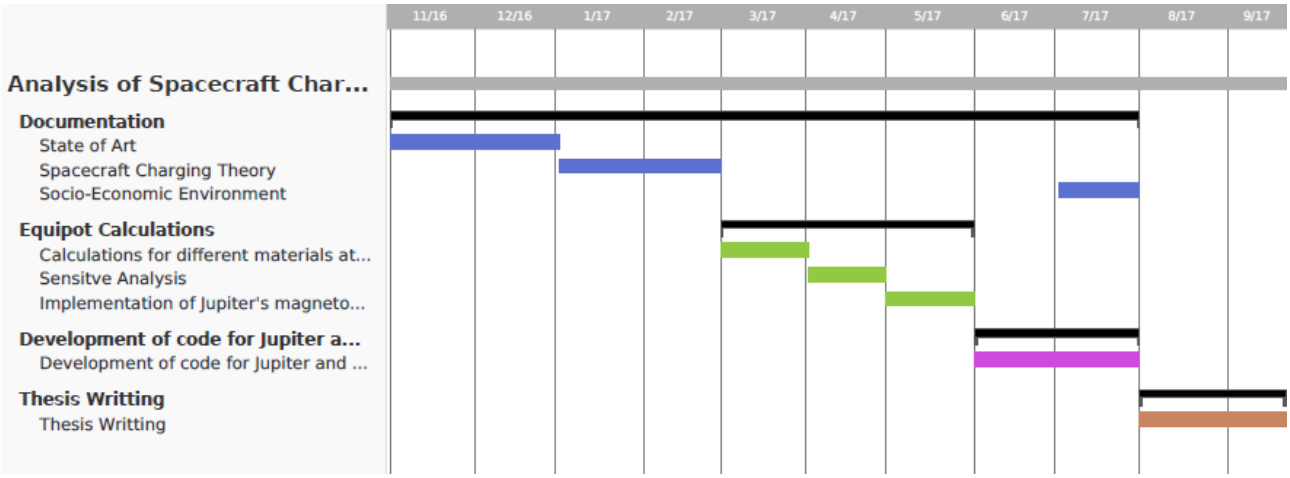

Figure 1.7: Gantt diagram for the project planning

1.6 Budget

Regarding the cost associated to this bachelor thesis, this last section is dedicated to present a provisional budget. In any engineering project, the budget is essential. It is important to remark that it is an approximation but not a real one.

1.6.1 Human Resources

The part of the budget dedicated to human resources correspond to the hours needed to the development of this bachelor thesis. The minimum number of hours associated to this project are the ones equivalent to 12 ECTS. Considering that 1 ECTS is equal to 25 hours, the minimum hours dedicated to this bachelor thesis are 300 hours. The minimum salary that a junior engineering must receiver per year is established in Article 33 of the Spanish "XVIII Convenio colectivo nacional de empresas de ingeniería y oficinas de estudios técnicos" [15]. It corresponds to 9.75€/h. Therefore, human resources have an estimates costs of €2925.

1.6.2 Software Cost

Two softwares have been used along this thesis: by one side, EQUIPOT code; by the other side, MatLab R2016b. EQUIPOT is a free software offered by ESA. Thus, its related costs are €0. Regarding MatLab software, it has a license cost of €2000. When doing this thesis, it has been a free license offered by Carlos III University. However, to make a realistic budget it has been considered the original price of the license. It would be interesting to include the cost of the operating system where these softwares were implemented. In this case, the OS in question is Windows 10 Home with a license cost of €135.

1.6.3 Hardware Cost

As this bachelor thesis is a theoretic one, the main tool used is a laptop with a cost of €800. Its depreciation period is considered of 5 years (60 months). As commented in previous section, this project last for 9 months where the laptop was a crucial tool. The imputable cost can be estimated in €133.33

Human Resources					
Category	Minimum number of hours		Total cost		
Junior Engineering	300		€2925		
Software					
Description	Quantity		Total cost		
Equipot	1		€0		
Matlab R2016b	1		€2000		
Windows 10	1		€135		
Hardware					
Description	Quatinty	Dedication	Depreciation period	Unitary cost	Imputable cost
Laptop	1	9 months	60 months	€800	€133.33
Total cost (without taxes)				€5193.33	
Indirect costs (20 %)				€1038.67	
VAT (21 %)				€1090.59	
TOTAL COSTS				€7322.59	

Table 1.2: Budget

1.6.4 Total Cost

As summary of this section, the total cost without taxes is the sum of the cost for human resources (€2925), the software cost (€2135), and the hardware cost(€133.23). All this contibution adds up to €5193.33.

Considering a 20% of indirect cost, (regarding time delays, software and hardware maintenance, securance of human resources, etc) and a 21% of VAT taxes, the total cost of this bachelor thesis is €7322,59.

Chapter 2

Spacecraft Charging

In previous chapter, it has been presented the effects produced when a spacecraft is electrically charged and why it is important to study them. In the following chapter, it is going to be introduced the physics concepts needed to apply in the study of the phenomenon. It is also important to know the state of art of this topic, what it has been studied and what it is being developed nowadays, and the regulation to be applied when these studies are performed.

2.1 Spacecraft Environments

The environment in which a spacecraft is submerged is a combination of the ambient and that one produced by the spacecraft itself. It can be characterized by four physical components:

- Neutral environment, which includes the ambient gas and gas released by spacecraft surface material, vented from spacecraft, or emitted during firings.
- Plasma environment. It includes the ambient plasma, that released by plasma thruster, that created by ionization, the one generated by arc discharges and that created by hypervelocity impacts with spacecraft.
- Radiation Environment, with electromagnetic and corpuscular components.
- Particle environment, consisting on ambient meteoroids, orbital debris and particles from the spacecraft.

The ambient space environment is usually a function of the orbit. The position with respect to the Earth is relevant for the spacecraft charging issue. There are five families of orbits, each one with a specific environment. The characteristics are described in Table 2.1. It is possible that a spacecraft would have a highly elliptical orbit that goes through all these five orbits. In this case, it is fundamental to analyze each orbit segment differently. As a summary, in figure 2.1 it is possible to see the level of charging hazard along the different orbits near The Earth.

The plasma environment is the dominant environment when it is talking about spacecraft charging [8]. To be more precise, the major plasma effects came from the slow accumulation of

Name	Atitude [km]	Inclination to equator [deg]	Description
Low Earth Orbit (LEO)	100-1000	<65	Cold, dense, ionospheric plasma; dense, supersonic neutral atmosphere; solar ultraviolet (uv); orbital debris;South Atlantic anomaly (SAA)
Medium Earth Orbit (MEO)	1000-36000	<65	Solar uv; trapped radiation belts; plasmasphere
Polar Orbit	>100	>65	Solar uv;cold, dense ionosphere; supersonic neutral atmosphere;orbital debris; auroral particles;solar flares; cosmic rays; SAA;horns of radiation belt
Geostationary Orbit	~ 36000	0	High-energy plasmasheet;substorm plasma; uv radiation;outer radiation belts;solar flares; cosmic rays
Interplanetary Orbits	Outside magnetosphere	N/A	Solar-wind plasma;solar flares; cosmic rays

Table 2.1: Classification of Earth's Orbits [8]

charge on surfaces. This accumulation of charged particle on surfaces produces electrostatic field that may provoke adverse interactions such ESD, material contamination due to particle deposition on surfaces, etc.

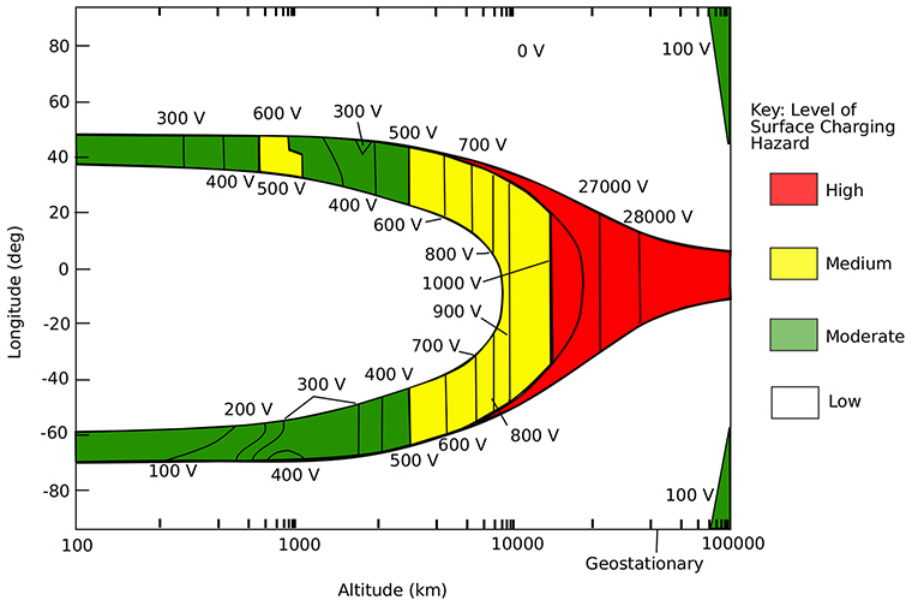

Figure 2.1: Levels of Surface Charging Hazard [16]

The intensity of this phenomenon depends on the location of the body, the material used, the local time and the space weather. All the previous variables are crucial when designing a spacecraft for a specific mission.

The electrical charging of a spacecraft has some related concerns which designers must care about:

- Surface Charging. Due to the accumulation of the charged particles on spacecraft surfaces.
- Internal Charging. Due to penetrating electrons.
- Current leakage. High voltage systems which can experience power loss.
- Environment modification. Produced by the particle emission by spacecraft surfaces. This provokes misleading in the measurements devices.

- Electric propulsion that creates a local plasma population and modifies the current balance of the satellite.

The focus of this bachelor thesis will be Surface Charging.

2.2 Surface Spacecraft Charging Theory

When designing a spacecraft, the objective of the study of this phenomenon is to know the final potential that this body will have when the equilibrium is reached. In this equilibrium situation, the total current to satellite is equal zero. This total current is split in several current contributions as functions of the potential V. Figure 2.2) is a graphical example of the different contributions to the surface charging. The basic equation expressing current balance for a given surface is:

$$I_T = [I_I(V) + I_{SE}(V) + I_{SI} + I_{BSE}(V) + I_{PH}(V) + I_C(V)] - I_E(V) \tag{2.1}$$

Where V is the satellite potential; I_E is the current produced by the incident electron on satellite surface; I_I the one produced by the incident ions on satellite surface; I_{SE} is the secondary electron current due to I_E; I_{SI}, the secondary electron current due to I_I; I_{BSE} is the backscattered electrons due to I_E; I_{PH} is the current produced by photoelectrons; and I_C is the conduction current. I_E and I_I are computed from the environment parameters. I_{BSE}, I_{SE} and I_{SI} are then determined using yield functions that will be defined later. I_{PH} is calculated from the material properties.

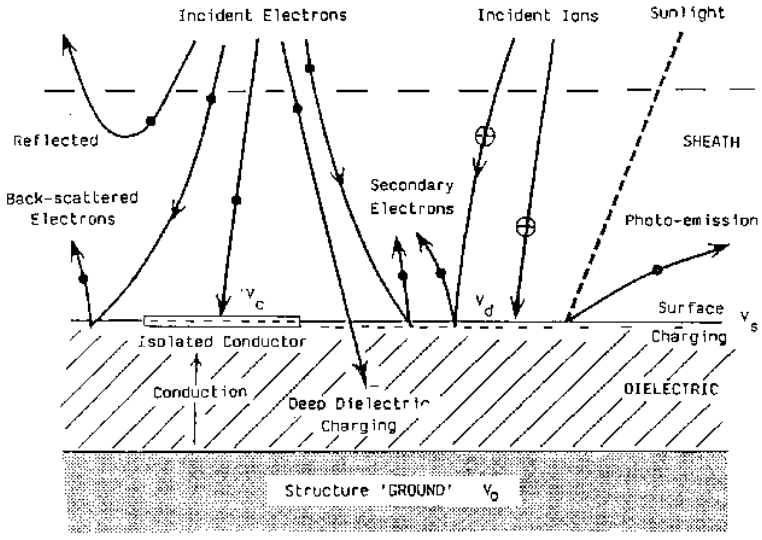

Figure 2.2: Current components to a surface on a spacecraft [14]

The charging process ends when the equilibrium is reached. The associated potential in this point is known as "floating potential". This equilibrium is dynamic and may vary with density of the current.

Spacecraft is considered to act as an isolated electrostatic probe that will collect charge adopting an electrostatic potential consistent with charge collection. Following this assumption, the

plasma associated with LEO and GEO must be treated differently. Usualy, the prevailing currents are both electron and ion current. Since the plasma density is low in GEO, the contribution of photoelectrons current in the current balance can be important. When the spacecraft is sunlit, the photoelectron became the prevailing current holding the potential in a small positive voltage; meanwhile in eclipse, the electron current is prevalent. Note that the contribution of photoelectron current depends on the material of the spacecraft's surface, the solar activity, the radiance incidence angle and the spacecraft potential bias.

Potentials on spacecraft are shielded from their surroundings in different ways depending on the characteristics of each plasma. A sheath is the region of space surrounding a body which feels a perturbation of potential caused by that body. It depends on the geometry of the body and the potential bias of the entire structure. This work will focus on spherical symmetry, which will be the approximated shape of the spacecraft considered here. The characteristic length that defines the size of the sheath is the Debye length. For not very high potential and spherical symmetry, this length is related with the potential as follows

$$V(r) = \frac{q \exp\left(\frac{-r}{\lambda_D}\right)}{r} \tag{2.2}$$

where λ_D is the so-called Debye length which is given by

$$\lambda_D = \sqrt{\frac{K_B T_e}{4\pi q^2 n}} \tag{2.3}$$

Being K_B the Boltzmann's constant, T_e is the electron Temperature (in Kelvin), q is the electron charge and n is the ambient plasma density. An approximated version of the Debye length in terms of the electron temperature T_e in electronvolts (eV) and the electron density in cm^{-3}

$$\lambda_D \approx 7.43\sqrt{\frac{T_e}{n}} \ \ [\mathrm{m}]\,. \tag{2.4}$$

Regarding these two last equations, Debye length varies with the plasma density and electron temperature; therefore, Debye length will vary along the different orbits already mentioned.

The classification into "thick" sheath and "thin" sheath came from determining whether λ_D is long (thick sheath) or short (thin sheath) compare to the spacecraft radius. For spherical symmetry, the sheath thickness can be estimated with the following expression:

$$S = \frac{1}{3}\left(\frac{2}{qK_B T}\right)^{\frac{1}{4}} (V_0)^{\frac{3}{4}} \left(\frac{1}{\pi n_0}\right)^{\frac{1}{2}} \left(\frac{1}{K^*}\right)^{\frac{1}{2}} \tag{2.5}$$

being V_0 the initial potential and where the parameter K^* can be found in ref. [8].

In LEO, Debye length is typically a few millimeters; it is considered the body is in thin sheath regime. Meanwhile in GEO, Debye length is typically tens of meters, much larger than the dimensions of the surface element or even the spacecraft; therefore, the body is in thick sheath regime.

2.2.1 Electron and Ion currents

With a small λ_D, the electron current is limited to the value corresponding for zero potential because the effective collecting area cannot increase. $I_E = I_{E0}$ and $I_I = I_{I0}$.

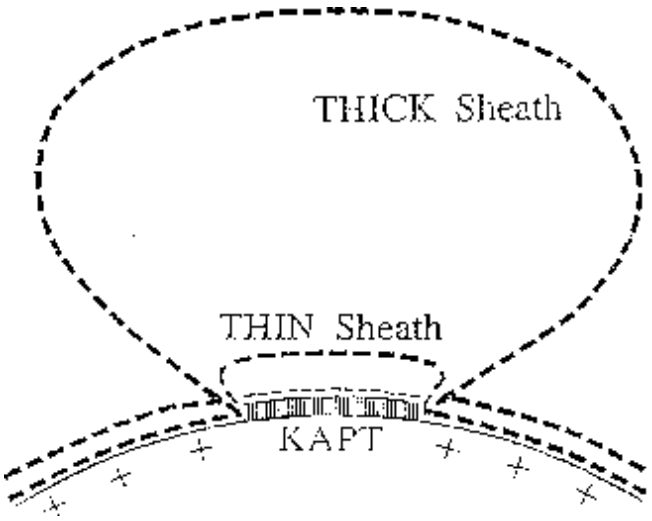

Figure 2.3: Schematic of thick and thin sheath growth on an isolated patch [17]

As it can be seen in figure 2.3, in the thick sheath the effective collecting area increases with potential. Considering a small spherical probe,

$$J_E = \begin{cases} J_{E0} \exp\left(\frac{qV}{E_E}\right) & \text{if } V < 0 \\ J_{EO}\left(1 + \frac{qV}{E_E}\right) & \text{if } V \geq 0 \end{cases} \tag{2.6}$$

where q is the magnitude of the electronic charge and E is the characteristic energy. Assuming an ideal thermal gas, it follows a Maxwellian distribution so $E = KT_E$. Temperatures are expressed here in eV, where 1 eV = 11605 K. The ion current I_I is defined with the same expression, but with a reversal of sign:

$$J_I = \begin{cases} J_{I0} \exp\left(\frac{-qV}{E_I}\right) & \text{if } V < 0 \\ J_{IO}\left(1 - \frac{qV}{E_I}\right) & \text{if } V \geq 0 \end{cases} \tag{2.7}$$

Although the expressions are nearly the same, the contribution of each element is very difference because J_I0 is much smaller than J_E0, because the current is inversely proportional to the square root of mass m. The expression for J_0 for a Maxwellian distribution with temperature T is

$$J_0 = \frac{qn}{2}\left(\frac{2K_B T}{\pi m_e}\right)^{0.5} \tag{2.8}$$

It is important to notice that, in order to set the voltage in eV, a factor of conversion should be included. From the energy relation which shows that $1\text{eV} = 1.79 \cdot 10^{-36} c^2$ Kgm^2/s^2 being c, the light velocity, equal to $3 \cdot 10^8$ m/s.

All these current components have units of flux [A/m^2]. The current is obtained by multiplying the area to the previous expressions.

2.2.2 Secondary Electron Currents

When an electron impacts on a surface, the material may reflect or absorb it. Inside the material, the electron may collide and "back-scatter" out of the material back into space. As the electron goes through the material, it loses energy and part of this energy can excite other electrons that may escape from the material [18]. Back-scattering is distinguished from true secondary emission by the energy of the emitted electrons, being the first ones those with the lower energy.

Secondary electron production involves the excitation of electrons within the material at a rate known as the "stopping power" of the material. This rate is proportional to the local energy loss rate by primary electrons. Secondary currents are determined using appropriate yield functions for incidence of flux that impacts the surface.

In this section, it is going to be presented the equations for the secondary electron currents used to make the study perform in this bachelor thesis. If the reader is interested in a deep reading of this topic, see [18], [19] and [20]

Backscatter electron current

As commented, it is necessary to find the appropriate yield function in such way that the expression for backscatter electron current $[A/m^2]$ become $J_{BS} = Y_{BS}J_E$. This yield, Y_{BS}, is a function of the electron energy at surface $E_s = E + qV$

$E_s(eV)$	Y_b
> 100000	0
10000 - 100000	$1 - 0.7358^{0.037Z}$
1000-10000	$1 - 0.7358^{0.037Z} + 0.1e^{\frac{E_s}{5000}}$
50-1000	$0.3338ln\left(\frac{E_s}{50}\right)\left[1 - 0.7358^{0.037Z} + 0.1e^{\frac{E_s}{50}}\right]$
< 50	0

Where Z is the atomic number. This yield-energy relation is obtained from [17]. The previous values are the yield function corresponding to normal incidence. For isotropic incidence, the value Y_BSn for normal incidence is transformed to

$$Y_{BSi} = 2\frac{1 - Y_{BSn} + Y_{BSn}lnY_{BSn})}{ln(Y_{BSn})^2} \tag{2.9}$$

Secondary electron emission due to protons

The process for SEE due to protons is similar to that one commented previously but instead of an electron which impacts the surface is a proton. In this case, the objective is to determine the yield function, Y_SI, that makes the relation $J_{SI} = Y_{SI}J_I$. This yield function is dependent of the angle of incidence of the proton beam. If there is a normal incidence, Y_{SI} is given by

$$Y_{SI} = Y_1 E_s^{0.5} \frac{1 + \frac{1}{E_m}}{1 + \frac{E_s}{E_m}} \tag{2.10}$$

where Y_1 is the yield at 1 keV and E_m is the energy for maximum yield.

For isotropic incidence, Y_{SI} is obtained from:

$$Y_{SI} = \left(2 - \frac{Q}{2}\right) 2^{-Q} Y_1 E_s^{0.5} \left(1 + \frac{E_s}{E_m}\right) \tag{2.11}$$

where

$Q = 0 for E_s > 10$
$Q = \frac{1}{E_s} - 0.1 for 0.476 < E_s < 10$
$Q = 2 for E_s < 0.476$

SEE due to electrons

Meanwhile SEE yield due to protons is a function of surface energy, $E_s = (E - qV)/1000$; SEE yield due to electrons is a similar function of surface energy but with opposite sign, $E_s = (E + qV)/1000$

According to Katz et al. [21], the importance of the accuracy of the secondary electron yields is decisive for the charging analysis. There are different models proposed to this study: Whipple-Dionne model, Sims model, Katz model, and Burke model for polymers are the most used. In this bachelor thesis, the 3 first have been applied and are going to be presented in a short way. If the reader has interest in a deeper study, read [18], [19], [20], and [22].

Whipple-Dionne's model [18] Dionne developed an expression that depends only on the primary energy and it is based in stopping power. The value obtained from this expression varies with the angle of incidence of electrons. For a normal incidence, the expression is reduced to:

$$Y_{SE} = 1.114 \left[1 - e^{-Q}\right] Y_m \left(\frac{E_m}{E_s}\right)^0 .35 \tag{2.12}$$

Where $Q = 2.28 \left(\frac{E_s}{E_m}\right)^{1.35}$ and Y_m is the maximum yield for maximum energy, E_m.

For an isotropic incidence, the expression gives an angle-averaged yield:

$$Y_{SE} = \frac{2.228 \left[Q - 1 + e^{-Q}\right]}{Q} Y_m \left(\frac{E_m}{E_s}\right)^{0.35} \tag{2.13}$$

Sims' model [19] Sims introduced in 1992 an expression for SEE yield based on Dionne and Burke models but with three free parameters: the maximum yield at normal incidence, the energy at maximum yield and the stopping power law index, n. As in previous model, it also has a dependence of the angle of incidence. Considering a normal incidence, the expression becomes

$$Y_{SE} = \frac{Y_m}{(1-e^{-x_m})}\left(\frac{E_m}{E_0}\right)^{n-1}\left(1-exp\left[-x_m\left(\frac{E_0}{E_m}\right)^n\right]\right) \tag{2.14}$$

Where n is the energy loss power and x_m is the dimensionless range at maximum yield:

$$x_m = \left(1-\frac{1}{n}\right)\left[e^{x_m}-1\right] \tag{2.15}$$

For a given value of n, x_m must be found by a numerical method. In our case, it will be solved with a Newton-Raphson iteration.

Regarding an isotropic incidence, the expression yields

$$Y_{SE} = \frac{Y_m}{(1-e^{-x_m})}\left(\frac{E_m}{E_0}\right)^{n-1} 2\frac{[x-e^{-x}-1]}{x} \tag{2.16}$$

Where $x = x_m\left(\frac{E_s}{E_m}\right)^n$

Katz's model [20]

Katz et al. in 1997 presented an expression similar to that one from Whipple-Dionne work. The principal difference is the formulation of stopping power, dE/dx, which includes an extra term in the power series expansion.

First, it defines an electron range, R, from which stopping power is evaluated. This range is defined by

$$R = r_1 E^{n_1} + r_2 E^{n_2} \tag{2.17}$$

Where r_1, r_2, n_1, n_2 are parameter which depend on the material.

Assuming stopping power to be linear in x, the expression to evaluate this term is

$$\frac{dE}{dx} = \left(\frac{dR}{dE_0}\right)^{-1} + \frac{d^2R}{dE_0^2}\left(\frac{dR}{dE_0}^{-3}\right)x \tag{2.18}$$

A maximum range, R_u, is calculated by making 2.18 equal to zero. This is solved through a quadratic equation root finding algorithm. Obtaining this maximum range, it is possible to get yield by using the following expression

$$Y_{SE}(E_s,\theta) = c_1\left(R_u\left(\frac{dR}{dE_s}\right)^{-1}\frac{\left[1-e^{-Q}\right]}{Q} + R_u^2 d^2\frac{R}{dE_s^2}\left(\frac{dR}{dE_s}\right)^{-3}\frac{\left[1-(Q+1)e^{-Q}\right]}{Q^2}\right) \tag{2.19}$$

where $Q = c_2 R_u \cos(\theta)$. For normal incidence, c_2 can be found by fitting $dY/dE = 0$ to E_m and later fitting $Y_{SE}(E_m)$ to Y_m to found c_1.

2.2.3 Photo-emission current

Regarding a sunlit spacecraft surface, the dominant component of equation 2.1 is the current due to the emission of photoelectrons. This emission occurs when solar photons impact the surface with enough energy to provoke electrons to escape. This photoemission will tend to hold the surface potential at a small positive voltage since that the number of photoelectrons that escape from the body is nearly equal to the number which does not.

The photoemission current is a function of the voltage, the temperature and the angle of incidence of the photons. The angle of incidence of the photons from the Sun with respect to the spacecraft surface reduces the photocurrent in proportion to its cosine. If the surface is positive, not all photo-electrons and secondary electrons will escape. In this case, the currents are reduced by a factor $\exp(-0.5V/T_S)$ where T_s is the effective temperature of emitted electrons. The temperatures are specified by Whipple in [18].

2.2.4 Conduction current

Conductivity current is a small fraction of the incident current. It plays a key role near the equilibrium, where other current components change very slowly with surface potential. Patch thickness, conductivity of the patch, temperature of the patch material and its relative permittivity are the four parameters which affect conduction current.

2.3 Surface Charging Codes

To find the charging state of a spacecraft, charging simulations are used. These simulations must have realistic representation of the different currents and the beam of electrons and ions that impacts the body. In Spacecraft Charging, the charging codes can be divided in 3 categories: Surface Charging, Internal Charging, and Environment model. In the following section, the codes used in the study of surface charging will be presented. Internal Charging and Environment model codes can be consulted at Appendix D of ESA standard ECSS-E-ST-20-06C [23]

As commented previously, the geometry of the body is essential for the study of surface charging. Therefore, simple 1-D codes can be used only as assessments meanwhile 3-D codes are needed for a real simulation.

The most common spacecraft charging code in use was NASCAP-GEO, a NASA-USAF charging analysis code. Lastly, ESA has sponsored the development of several modelling codes such Equipot and SPIS that are publicly available for all users.

2.3.1 NASCAP Family of Charging Codes

- NASCAP-GEO [24] This code is used for simulating surface charging in the outer magnetosphere. It is a 3-D code that uses a two-Maxwellian environment for both ions and electrons

for calculating the current contributions. It uses an iterative process that obtains total current and potential until equilibrium is reached.

- MATCHG [24]. It is a simple 1-D code based on a subset of NASCAP subroutines. It uses "thick sheath" approximation. This is useful at GEO but for charging in low-altitude conditions, another code must be used.

- NASCAP-LEO It is used at low-altitudes. This code has a better geometrical model than NASCAP-GEO, meanwhile it does not simulate spacecraft sheath with accuracy. It used normally for the simulation of parasitic currents from high potential surfaces.

- NASCAP-2K. The most recent NASCAP code, it is a combination of the capabilities of previous codes with a realistic geometry.

2.3.2 Equipot

Equipot [17] is a code implemented in SPENVIS website. It assumes a spherical geometry and allows to estimate the differential charging between a patch and the ground structure. Equipot is applicable to GEO and LEO charging because it can assume thin or thick sheath current collection. It is used as a first assessment. This bachelor thesis will be focus on this charging code in the following sections.

2.3.3 PicUp3D

PicUp3D is a 3D particle-in-cell (PIC) code that performs an exact computation of the sheath structure and of the current collected by spacecraft surfaces. However, other surface interactions that photo-electron emission are not considered.

2.3.4 SPIS

This code is much similar to PicUp3D with the capability of calculating a large class of surface interactions (photo-electron emission, SEE, backscattering, etc.).

2.3.5 POLAR charging code

POLAR code has been design for the assessment of sheath and wake effects on Polar orbiting spacecraft. Spacecraft velocity is included and one or two Maxwellian components may be used to define the ambient plasma. Its process of calculation is alike NASCAP.

2.3.6 Multi-Utility Spacecraft Charging Analysis Tool (MUSCAT)

MUSCAT is a code designed by the Japan Aerospace Exploration Agency (JAXA). It is a tool for analyzing spacecraft charging in different environments at LEO, GEO and interplanetary regions. It was developed in 2004.

2.3.7 Coulomb code

This code uses the Langmuir equations to determine the primary currents of plasma particles with a 3D geometry. It is a Russian tool developed in 1996. [25]

2.4 Mitigation Techniques

In most of the cases, spacecraft charging is a hazard that must to be reduced when it is not possible to be avoided. This reduction could be performed by mitigation (method or design that makes this issue less severe). It would be preferable that the mitigation was performed by means of prevention. Spacecraft surface potential could be prevented or reduced by changing materials, conditions and environments. However, prevention is not always possible due to the unexpected changes in the space environments and the properties of the surface material. Once prevention methods were included in the design of a spacecraft and the hazard is still important, the mitigation techniques must be introduced in the design.

Nowadays, the mitigation techniques are one of the most important studies in development. In 2003, Lai presented an overview of the technique methods in used at that time [26]. In 2012, it was published guide to mitigating spacecraft charging effects [16] that provides some guidelines in terms of mitigation spacecraft effect for designing a spacecraft.

Sometimes, the bodies that have high potentials need large times to be charged at these values. Consequently, it is possible to implement mitigation methods that compensate the charging effect after the equilibrium potential is reached. Considering spacecraft as a spherical conductive surface, the charging with a radius R (cm) and a charging current density J (A/cm^2), the time needed to charge the body at a potential V is

$$\tau = \frac{C_\infty V}{4\pi R^2 J} \tag{2.20}$$

where C_∞ is the capacitance of the spacecraft with respect to infinity. This parameter for a spherical symmetry is given by $C_\infty = 4\pi\epsilon_0 R$; being ϵ_0 the dielectric permittivity in vacuum [27].

In general, there are two types of spacecraft charging mitigation methods. When it is automatic, the technique is considered as a passive one. By contrast, if it is controlled by commands, the method is an active one. The most common mitigation techniques are presented in the next subsections. There is no need of command or control to use this method, therefore is a passive method. The disadvantage that this method have is that the electron emission is only produced from the conducting ground.

2.4.1 Passive Methods

Sharp Spike

Very high electric fields are generated by sharp spikes protruding from charged surfaces. This high electric fields produces an emission of electrons which only reduces the negative potential of the ground surface connected to the spike. Differential charging can occur. Spike tip should be protected by means of ceramic coating in order to mitigate sputtering. See figure 2.4.

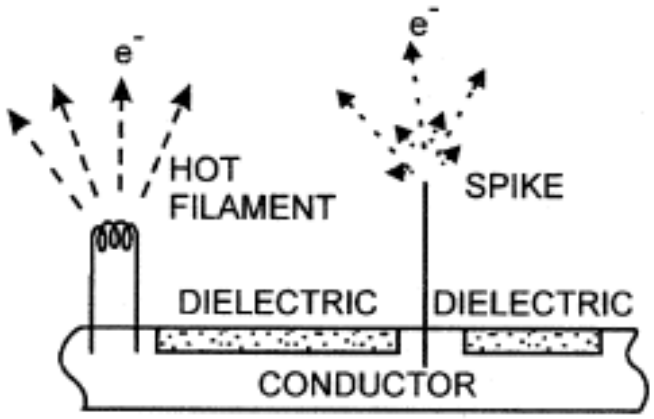

Figure 2.4: Electron emissions from a sharp spike and a hot filament [26]

Conducting Grids

Conducting grids method is to cover a nonconducting surface with a mesh of conducting wires. It is not a recommended method for most cases because the wire mesh provides a uniform potential and periodic potential differences may appear.

SemiConducting Paint

To eliminate the periodic potential problem produced by previous method, it is used conducting paint. It produces an increase of conductivity on dielectric surfaces, so it provides mitigation for dielectric surface charging issue.

High Secondary Electron Yield Material

The secondary electron yield $\delta(E)$ increases with the primary electron energy until it reaches $\delta_{max}(E)$. For higher energies, the excited electrons are deep inside the solid and they have not sufficiently

energy to escape; therefore $\delta(E)$ decreases. The use of coating of high secondary electron emission coefficient would work until the energy is high enough to produce $\delta_{max}(E)$ less than unity when there is no protection against charging. This technique mitigates for primary electrons at energies between the [$\delta(E)$=1] crossing points only.

2.4.2 Active Methods

Hot-Filament Emission Method

Hot filament emission method consists on emitting electrons from hot filament which are not melting. The process of mitigation is very similar to Sharp Spike one. As in the other case, electron emission from hot filament can reduce the potential of the ground surface but not the dielectric surfaces. Differential charging may appear in both cases. See figure 2.4. The current emitted may be limited very near the filament, because the energy of thermal electrons is low.

Electron and Ion Beam

This is an active method that consist in the emission of low-energy positive ions from a highly negatively charged spacecraft. These ions have not enough energy to go very far and they have to return to spacecraft. The potential can be mitigated up it reaches the initial energy of the ions emitted from the spacecraft.

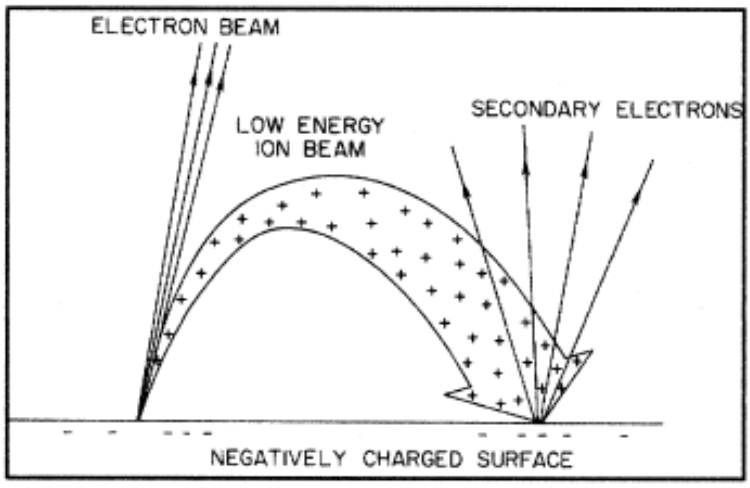

Figure 2.5: Emission of electrons and ions from a negatively charged surface. The ions return; the electrons leave [26]

The emission of electrons mitigates only conducting ground charging and it appears differential charging issues.

Plasma Emission

Plasma emission is a mixture of low-energy ions and electrons that combines the advantage of both method. This technique has been demonstrated by the charge control experiment on the DSCS satellite. The results of this experiment shown that it worked.

Evaporation

It is known that polar molecules attach electrons. This method consist on spraying polar-molecule liquid droplets all over the spacecraft. Electrons will be attached to polar liquid on the spacecraft surfaces. When this liquid evaporates, take away the excess electrons and reduce surface potential. The technique mitigates metals and dielectric surfaces, reducing differential charging.

Mitigation techniques are one of the most critical issues in the study of spacecraft charging area. The already mentioned methods are some examples of these techniques. Since this bachelor thesis is not oriented to this topic, it would not be presented a deep study about it. If the reader wants to know more about mitigation techniques, the reading of "Guide to Mitigating Spacecraft Charging Effects" book would be a good initial point.

2.5 State of Art

In 1981, Garrett presented a review about the charging of spacecraft surfaces [28]. The development of the spacecraft charging was divided in four phases.

The first studies of this effect appear in 1924 with the probe work of Langmuir [29]. Considering the vehicle as a probe is the basis of the theory of this spacecraft charging. In this first phase, it was developed the probe theory. In addition, with the advent of the rocket, new areas appeared. In early 50's, spacecraft charging emerged as a discipline. One of the first paper that presents spacecraft charging effects was published in 1955 by Johnson and Meadows [30].

In 1957, the studies about the distribution of charge (or sheath) around a vehicle begin to be considered. A second phase of spacecraft charging studies began. Along this phase, it also was considered the effect of electric field induced by the movement of a satellite across the Earth's magnetic field. In the early 60's, the first satellites with potential measurements were launched. The first one was Sputnik 3 in 1959 [31]. The second phase finished with the first review of spacecraft charging in 1961 published by Chopra [32]. At that time, the theory for spacecraft charging has been stated. Preliminary observations by satellites and rockets were proved that this effect existed and that the photoemission and ambient electron flux were recognized as dominant sources.

The third phase begin a little earlier than 1961 with the studies of Bernstein and Rabinowitz [33] referring to spherical and cylindrical probes inmersed within low-density plasmas. In 1961, Davis and Harris [34] calculated the shieding of a rapidly moving sphere in ionosphere. Their results were consistent with Explorer 8 measurements. It was the first accurate measurements at high altitude. Along this phase, more studies that predict measurements obtained from satellite were presented. The most complete works of this period probably were the first book concerning this

topic [35] and the thesis of Whipple [36]. This thesis established the basic components of current charging theory and the range of the observations, and marked the end of the third phase in 1965.

The fourth phase was characterized for the increment of more sophisticated models in situ measurements and the definition of some plasma environments. During this phase, the SCATHA (Spacecraft Charging At High Altitude) satellite mission occurred. With the analysis of the data obtained from this mission by Mullen [37] and the reviews about this topic by Whipple [18] and by Garrett [28] ended 20 years of spacecraft charging studies. The implications of all the findings along this period were summarized in the NASA Spacecraft Charging Design Guidelines [38] and MIL STD 1541A [39].

In 2000, Garrett published an update of its initial review [40]. In this paper, it is presented the fifth phase as the period between 1980 and 2000. The studies about the deep internal charging instead surface charging characterized this last phase. This period it is also characterized by the development of the first spacecraft charging tools. In 1978, NASCAP tool were presented. This was the most common tool used to the simulation of spacecraft charging models. In the 90's, tools like Equipot and Coulomb were presented in order to introduced more user-friendly codes. In the last years of XX century and the first decade of XXI century, these codes were improved, new ones were presented (like MUSCAT tool) and as happened in the theoretical works, it appeared the deep internal charging tools.

Nowadays, there exits new frontiers in the spacecraft charging theory development. In 2012, Ferguson published a paper about that for the 11th Spacecraft Charging Technology Conference [41]. Non-static material properties, non-static charging models, novel mitigation techniques, and new technologies and power requirements were the four new frontiers stated by Ferguson. The idea is that the new studies verse about one of this topic in terms of spacecraft charging.

Last year, the 14th Spacecraft Charging Technology Conference took place in Noordwijk, the Netherlands. On this occasion, the agencies presented their overviews about this topic.

Within the ESA program, there are several missions currently being developed like JUICE mission designated to study plasma in Jupiter's satellites. The use of SPIS has become common within Europe and it is constantly improved. It is being developed a new internal charging software called Elshield. Regarding instrument development, some new instrument has been developed as the HOPE-M plasma instrument which has been prototyped and tested in laboratory. It also some new charging environment definition were stated. [42]

Spacecraft charging continues to be a strong area of research and development in the United States. In terms of flight experiments and on-orbit measurements, it is necessary to highlight JUNO mission that arrived at Jupiter in July 2016 and Cassini-Huygens mission that launched in 1997 and that has finished in September 2017. JUNO mission will perform measurements of jovian radiations and charging environment among other experiments. Cassini-Huygens mission after 20 years of observation orbiting Saturn and its satellites. Within the diverse experiments and observations it made, one of them is to provide about the magnetic field and plasma parameters of the saturnian magnetosphere. US has focused on development of terrestrial and jovian environments by different agencies. Jet Propulsion Laboratory (JPL) from NASA continues to update radiation belts from planets like Jupiter, Saturn, and Uranus. [43]

In Japan, many activities related with spacecraft charging are performed. The already pub-

lished "Satellite Design Guideline for Charging and Discharge" (JERG-2-211) has been revised and updated with new measuring material data and the use of charging tools. JAXA has several satellites that perform on-orbit measurements and Kounotori Integrated Tether Experiment (KITE) is in progress.

Finally, other countries like Russia and China presented in this conference their activities about this research area. Russia is focusing in the development of mitigation techniques, on-orbit measurements and internal charging issues. China became to pay attention to spacecraft charging recently with the launch of many satellites at geosynchronous orbits.

2.6 Standards and legal framework

Due to the importance of avoiding spacecraft charging, many documents and standard were proposed to set some design guidelines. As the research was performed at the different space agencies in the world, many of them have their own standards and handbook proposed.

2.6.1 NASA documents

The most remarkable documents about spacecraft charging design guidelines and standard published by NASA are:

- **NASA-STD-4005** Low Earth Orbit Spacecraft Charging Design Standard. It is a standard document focused in LEO and provides requirements to various plasma interactions. [44]
- **NASA-HDBK-4002-A** Mitigating In-Space Charging Effects —A Guideline. [45] This document describes conditions where spacecraft charging becomes a hazard and list design solutions. It is intended to be an engineering handbook.
- **NASA-HDBK-4006** Low Earth Orbit Spacecraft Charging Design Handbook. [46] This document is a handbook that provide design guidance referenced in NASA-STD-4005.

In Europe, there exits the European Cooperation for Space Standardization (ECSS). The main purpose of this initiative is to develop a single set of standards in all European space activities. The documents are available at ESA-ECSS website, http://www.ecss.nl. Within this site, it is possible to check the currently active standards and handbooks. These documents are important because they present the issue to be solved, the design requirements imposed for the mission safety and theoretical approach to the issue. Regarding Spacecraft Charging there are two important documents:

- **ECSS-E-ST-20-06C** Spacecraft charging standard [23]. This document published in 2008 provides instructions to identify the spacecraft charging issues and to take measures in order to avoid and minimize hazard effects. It also gives technical information about the spacecraft charging process.

- **ECSS-E-ST-10-04C** Space Environment [47]. This standard defines the natural environment for all space regimes. It also presents models and rules for finding the local induced environment.

Regarding ESA documents, Rodgers et al. presented in 2016 a study about the need of review these spacecraft charging standards [48].

The presented documents can be considered the most used standards and handbooks when designing a body in terms of spacecraft charging. In addition to them, there exists standard published by other agencies like JAXA which presented spacecraft standard JERG-2-211A in 2012 [49].

Chapter 3

Equipot

As it can be seen in previous sections, the effects of the spacecraft charging can be a factor of risk to be taken into account. For this reason, it is crucial to perform simulations studying this problem during the design of a spacecraft. The simulations are useful only if they can obtain realistic values of the different parameters that affect the spacecraft charging.

In the previous chapter, the different codes used to perform surface charging simulations were presented. As mentioned, this bachelor thesis is focused in the study and performing of Equipot Code. In this chapter, Equipot is going to be presented as a charging code. Later, it will be done a comparison between a sensitive analysis perform in 1989 by Sims and Wrenn [14] and other one performed in 2017 by the author of this thesis. Finally, it is going to be presented a study about how the equilibrium potential is varied for different materials at fixed environment and for one material at different environments.

3.1 Description of Equipot charging code

EQUIPOT is a simulation code for spacecraft charging analysis which was implemented in the SPENVIS program.[1] This code offers a rapid assessment of surface charging on a spacecraft. To make easier and faster the simulation, EQUIPOT assumes a very simple model: a spherical spacecraft with an isolated patch of material. It calculates the different components of current to both surface and patch and estimates the voltage needed to achieve zero net current.

Two main set of inputs are required to run EQUIPOT: the plasma environment and the spacecraft material. The first input can be selected from a range of pre-defined environments already included in the basis of the program (See table 3.1) or the user can manually introduce the parameters desired. The second one has also predefined parameters that can also be user modified.

Regarding the plasma environment, the parameters are specified by defining the thermal spectra and energy spectra. EQUIPOT offers the possibility of submitting three thermal spectra for electrons and ions, one electron flux spectrum and three ion flux spectra.

[1] SPENVIS is an online tool intended to facilitate the uses of models of the spatial environment. [50]

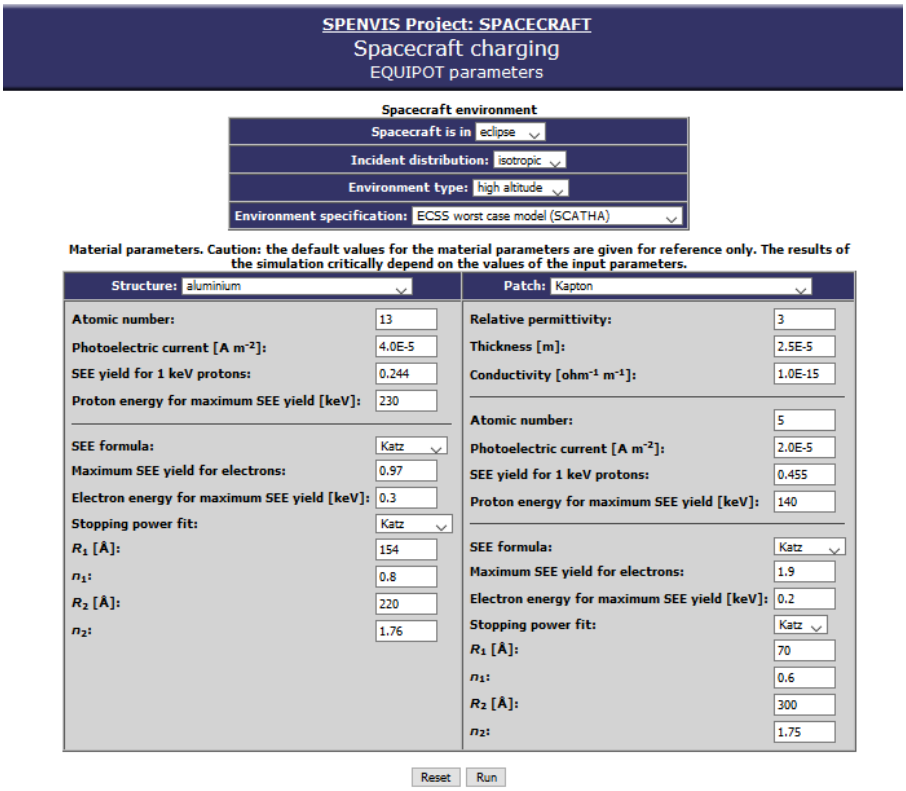

Figure 3.1: EQUIPOT interface [17]

Description
Low altitude environments
IRI at solar minimum, in winter, at 800 km, plus 10 kR aurora
IRI at solar maximum, in summer, at 800 km, plus 10 kR aurora
Maxwellians for 1,000 km plus aurora
Auroral type spectra from DMSP
Cold Maxwellians for ram test
Test spectra and Maxwellians
Cold Single Maxwellian and Fontheim electrons
High altitude environments
ECSS worst case model (SCATHA)
NASA guidelines worst case
NASA guidelines average GEO environment
Meteosat very disturbed
Meteosat very quiet

Table 3.1: Pre-defined environments in Equipot [17]

Considering the materials, they can be selected both for the structure and the patch. Materials are determined by nine parameters which are a subset of the NASCAP parameter set The default values are provided by ESA SPINE (Spacecraft Plasma Interactions Network in Europe). They can be modified by the user or a new material can be defined.

As commented previously, the secondary electron emission yield function plays a very important role in the computation of equilibrium potential. Therefore, the selection of the secondary emission yield model is crucial for the simulation. EQUIPOT supports three models for all the materials: The Katz model [20], the Whipple/Dionne model [18] and the Sims model [19]. It also provides the Burke model [22] for polymers. The spacecraft geometry is assumed to be a sphere with radius of 1 m with a planar patch.

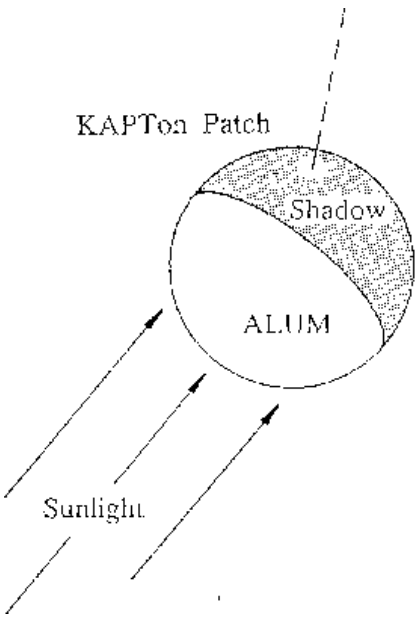

Figure 3.2: Geometry used by EQUIPOT [14]

The idea for the implementation of EQUIPOT is that the numerical methods ought to be as simple as possible and the run times should be consistent with an interactive code. Consequently, it uses a simple voltage stepping algorithm that controls the direction and increment to minimize the net current and locate equilibrium by assuming a single root solution. (See 3.4) Voltage is multiplied by a factor of 10 until J_{net} changes the sign. At this point, voltage step is reduced by a factor of ten, a new loop is initiated and continued until equilibrium is reached.

Once the code is run, the code offers diverse ways to represent the results:

By one side, the input data and results obtained are shown in one .csv file and in HTML code.

By other side, it is possible to plot the results. The options to plot are varied. The user can choose the different plots depending on his interests: the electron emission yield (for the structure of the patch), how change different parameters (voltage, net current, photoelectron current, etc.) with time, and how change the diverse fluxes with energy. Figure 3.3 is an example of mentioned interface.

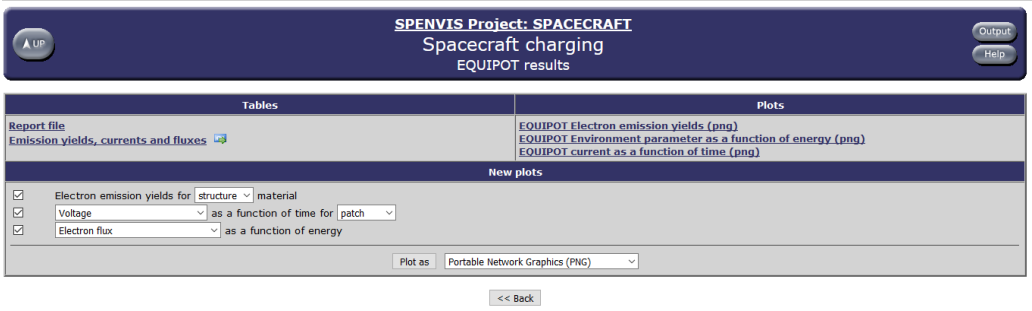

Figure 3.3: EQUIPOT results interface [17]

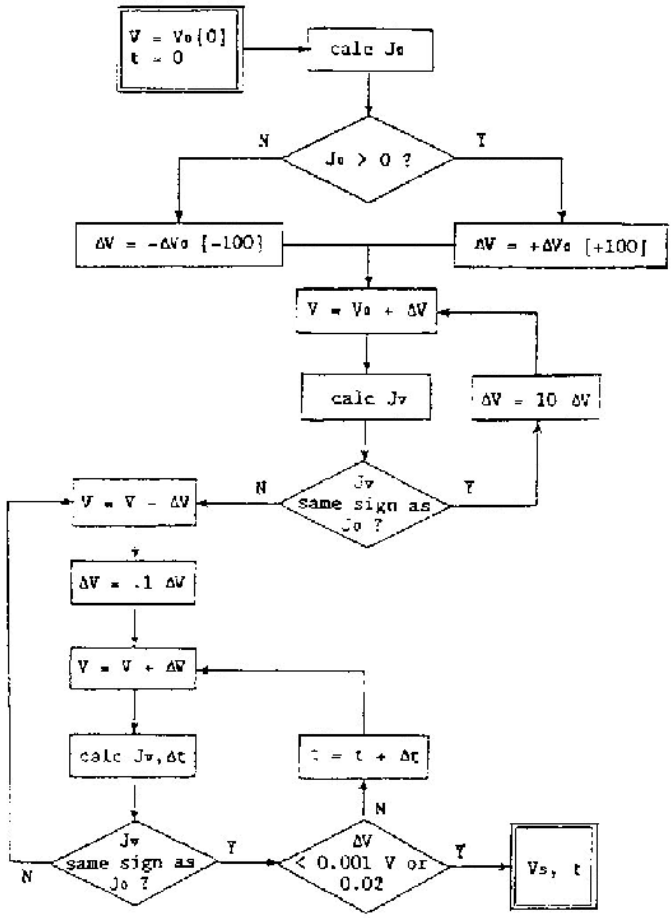

Figure 3.4: Voltage stepping algorithm used by EQUIPOT [14]

3.2 Sensitivity Analysis

In 1989, Sims and Wrenn performed a sensitivity analysis of the surface charging of a spacecraft with the EQUIPOT code [14]. This code is an interactive tool and the pre-defined parameters are obtained from the ESA database. As the space environment changes with time, it also does this

database so the reference data used for the sensitivity analysis in 1989 are not the same that those one that are used nowadays. Note that in 1990 a maximum of solar irradiance was occurred within the 11-year solar cycle.

The data the most affected for these changes is the one related with the pre-defined environments. The mainly reason is the change in the solar cycle [2] . When the sensitivity analysis was performed, it was the solar cycle 22 meanwhile today the current solar cycle is 24 which begun in 2008, with a minimum of solar flux.

In order to get a deep knowledge of the tool, it was considered performing again the sensitivity analysis would be interesting. The aim of this section is to present what was done by Sims and Wrenn and the new contributions that have been done to this study.

The initial study was performed following some assumptions:

- The structure is sunlit
- The spacecraft surface is made of aluminum and the patch, of Kapton.

The surfaces properties of the Kapton are given below.

Thickness: 25 μm

Relative permittivity: 3.0

Conductivity: 1.0E-15 mho/m

Atomic number: 5.0

Maximum normal SEE yield: 1.9

Energy at maximum normal SEE yield: 0.20 keV

Yield of 1 keV protons: 0.455

Energy at maximum proton yield: 140.0 keV

Photelectron yield: 2.0E-5 $Am^{-}2$

The aim of this study was to analyse how is the change in the equilibrium potential if the parameters on this list are varied. In the study performed by Sims and Wrenn the environment chosen was a variation of the worst-case SCATHA environment [37]. It was modified to obtain a potential of -10 kV for the definition of Kapton corresponding to the previous material parameters. In this analysis, the environment chosen was the worst SCATHA one that is predefined in the EQUIPOT tool. The values for the parameters defining SCATHA double maxwellian environment for the both analysis is shown in tables 3.2 and 3.3. In case of the first analysis, the envrionment is defined by a double maxwellian distribution with an additional cold plasma component. The equilibrium potential obtained for this case is -10.5 keV. Finally, the last two assumptions in order to obtain these values of the potential are isotropic particle incidence and the Katz model of secondary electron emission is used.

[2]The amount of magnetic flux that rises to the Sun's surface varies with time in a cycle called the solar cycle. This cycle lasts 11 years on average.

	1989 Study			
	Electron Density [cm^{-3}]	Electron Temperature [keV]	Ion Density [cm^{-3}]	Ion Temperature [keV]
Hot Plasma	2.1	26	0.7	25
Cold Plasma 1	0.9	0.6	1	1
Cold Plasma 2	0.1	1	0.1	1

Table 3.2: Parameters defining SCATHA worst environment in Sims and Wrenn's study

	2017 Study			
	Electron Density [cm^{-3}]	Electron Temperature [keV]	Ion Density [cm^{-3}]	Ion Temperature [keV]
Hot Plasma	1.2	27.5	1.3	28
Cold Plasma	1	0.2	0.6	0.2

Table 3.3: Parameters defining SCATHA worst environment in 2017 Study

3.2.1 Variation of parameters affecting the conduction current

As commented in chapter 2, the conduction current depends on four parameters: the patch thickness, the conduction of the patch, the temperature of patch material and its relative permittivity. The Equipot code allows to change all of them but not temperature of patch material. In the analysis previously mentioned, only the thickness and the bulk conductivity were changed as well as in this new analysis.

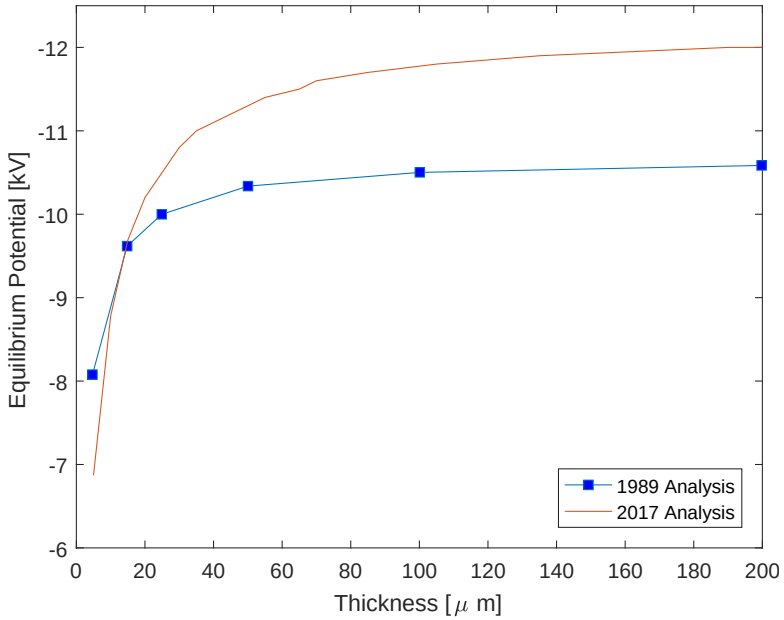

Figure 3.5: Equilibrium potential as a function of kapton thickness

Thickness has been varied from 5 μm to 200 μm. The figure 3.5 shows the effect of the thickness in the equilibrium potential for the two analyses. In the first one, the more significant changes are appreciated for thickness below 50 μm. For higher values of the thickness, the equilibrium can be considered nearly constant. The variation of the thickness for the analysis perform in 2017 is represented by the red line. In this last case, the change in equilibrium potential is more marked for thickness below 60 μm. In contrast to the Wrenn and Sims' study, for values higher 60 μm up

to near 100 μm the change of potential is still noticeable. It is important to comment that the change in potential is bigger in the second analysis, varying from about -6.9 keV to near -11.5 keV (a difference of 4 keV, finding a difference of about 2.5 keV in the other case).

As it was exposed previously, the maximum point of solar flux in the cycle 22 occurred in 1989 while the solar flux in 2017 is at minimum of the cycle. It should be expected that the equilibrium potential was higher for the case of Wrenn and Sims' analysis due to this solar activity, increasing the effect of photoelectrons. Indeed, it does happen for thickness below 20 μm. However, for higher thickness values the equilibrium potential is reached at higher potential in the 2017 analysis case here presented.

Regarding the bulk conductivity, it is reduced from 10^{-14} to 10^{-16} mho/m. The only comment about this parameter observed by Wrenn and Sims was that "the significant change resulting from making Kapton slightly more conductive is evident". In figure 3.6 the results from the two analyses are shown. Two aspects ought to be commented in this figure. By one side, the resulting change is even more significant than expected. By the other side, it is interesting to remark that at 10^{-16} mho/m the body is expected to be more charged nowadays; meanwhile if the conductivity is increases, this situation is inverted.

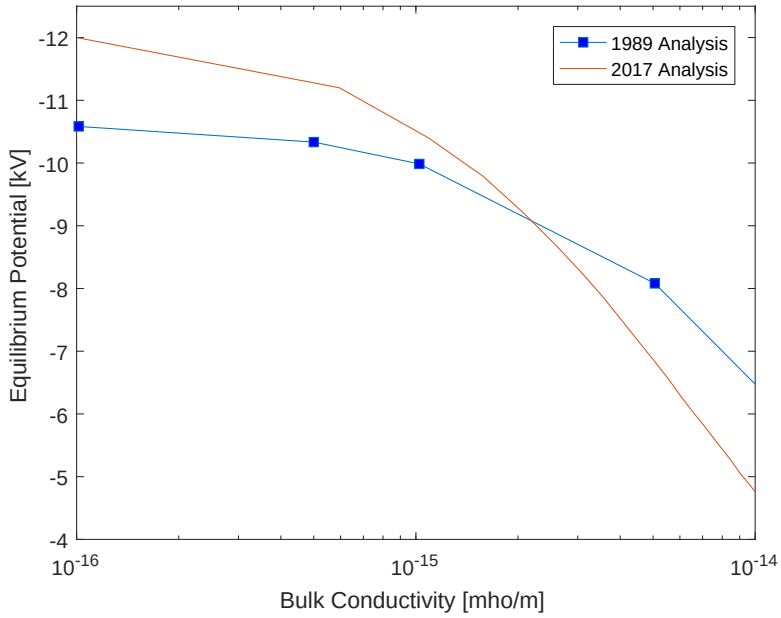

Figure 3.6: Equilibrium potential as a function of the bulk conductivity of kapton

3.2.2 Variation in the photoelectric yield current

The photoelectric yield current is only present in the balance equation when the body is sunlit which is one of the environment conditions imposed in these two studies. To illuminate the Kapton patch at oblique angles of incidence was though as to be instructive. Currently, the code allows to introduce the sun angle directly in degrees. In 1989, this angle had to be introduced in terms of its cosine. As it is possible to see in figure 3.7, it has been analysed the equilibrium potential varying the illumination angle from complete shadow (normal incidence, 90º) to near 72º. This

range was chosen at first experiment because they determined that at 72º the negative charging was completely prevented by the current of photoelectrons. However, in the most recently one, this component could prevent this negative charging up to 80º, which is near fully shadow.

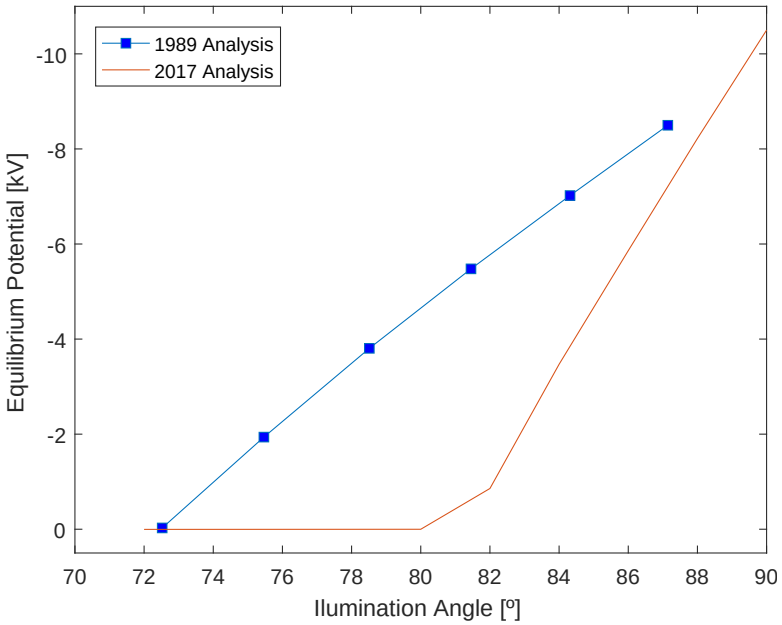

Figure 3.7: Equilibrium potential as a function of illumination angle for a kapton surface

3.2.3 Variation of SEE current for isotropic particle incidence

An isotropic flux tends to increase the value of the maximum secondary electron emission yield and moves its position to a higher energy [18]. The three models used by Equipot to calculate SEE current include an expression which correct for isotropic incidence. User must input the values for normal incidence and then the Equipot make the conversion if "isotropic" tag is selected. Table 3.4 shows the parameters defining the isotropic SEE yield function with the input values submitted by the user and the position of the peaks in the corrected models.

SEE model	$d_{max,input}$	$E_{max,input}$ [eV]	$d_{max,isotropic}$	$E_{max,isotropic}$ [eV]
Katz et al, [20]	1.9	200	2.7434	316.23
Whipple [18]	1.9	200	2.76630	316.23
Sims [19]	1.9	200	2.4982	316.23

Table 3.4: Parameters defining the isotropic SEE yield function

Only the two first SEE model were used in the analysis of Wrenn and Sims. In 1992, Sims introduced a new SEE model that is currently available at Equipot Code. It has been considered as a good point to include the study of this model with respect of the other ones that had already been compared. Figure 3.8a shows the full SEE curves presented in the first analysis. Figure 3.8b shows the full SEE curves of the three models that has been obtained for the new analysis.

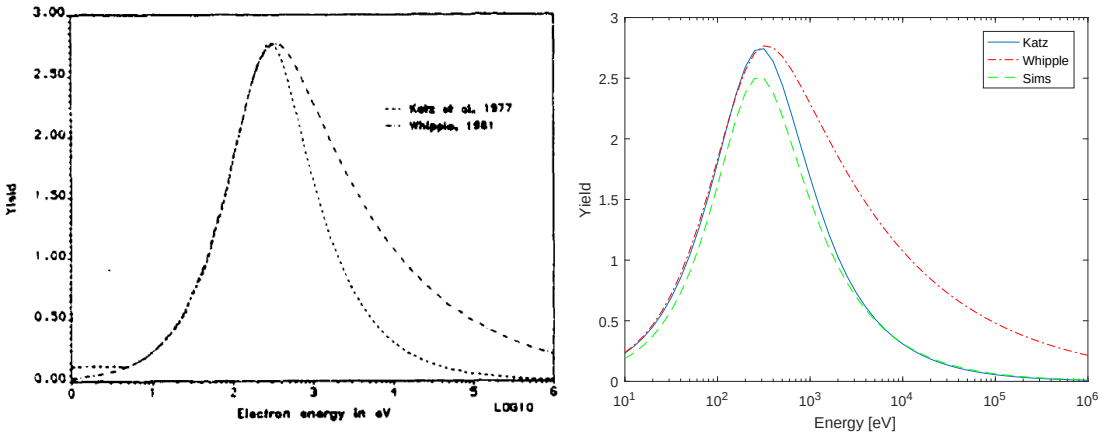

(a) SEE curves from the 1989 analysis [14]

(b) SEE curves from the 2017 analysis

Figure 3.8: Secondary electrons yield for Kapton; isotropic particle incidence

The conclusion in the first study was that the peak positions were in good agreement but the main difference was at high incident energies. When comparing three models, it is possible to see that the peak positions for the Katz and Whipple model are nearly coincident. However, the peak position for Sims model is lower. In contrast, Katz and Sims models have pretty similar results at high energies.

Following the sensitive analysis, the maximum yield and the maximum energy have varied in order to see how equilibrium potential is affected by these changes. Tables 3.5, 3.6, and 3.7 show the results of this variations for the three models with this new study. The conclusion obtained in the first analysis, for Katz model, since the amount of change of the position of the peak was small, the equilibrium potential was affected only slightly (less than 2%). Meanwhile, the Whipple model has two points to mention: the potential is significantly different from results obtained with the Katz model; and that the equilibrium potential is much more sensitive to minor changes in the peak position.

	d_{max}	E_{max} [eV]	Voltage [V]
default	2.7434	316.23	$-10.5 \cdot 10^3$
$d_{max} + 10\%$	3.0178	316.23	$-10.4 \cdot 10^3$
$d_{max} - 10\%$	2.4691	316.23	$-10.7 \cdot 10^3$
$E_{max} + 10\%$	2.7434	347.85	$-10.5 \cdot 10^3$
$E_{max} - 10\%$	2.7434	284.61	$-10.6 \cdot 10^3$

Table 3.5: Results of variation in the isotropic Katz expression. 2017

In the second analysis, these statements are fulfilled. Meanwhile the variation of potential in both Katz and Sims models is slight, in the Whipple model has a considerable impact. It also noticeable that, as in the previous study, the difference in magnitude of the potential between Katz and Whipple are something to take care about. In terms of equilibrium potential, it can be considered that Katz and Sims models have results nearly equal; being the Whipple model the most dissimilar one.

With this parameter variation, it is not the intention of the author to make statement about

	d_{max}	E_{max} [eV]	Voltage [V]
default	2.7663	316.23	$9.85 \cdot 10^{-2}$
$d_{max} + 10\%$	3.0429	316.23	$4.58 \cdot 10^{-1}$
$d_{max} - 10\%$	2.4897	316.23	$-2.56 \cdot 10^{3}$
$E_{max} + 10\%$	2.7663	347.85	$2.18 \cdot 10^{-1}$
$E_{max} - 10\%$	2.7663	284.61	$-1.34 \cdot 10^{3}$

Table 3.6: Results of variation in the isotropic Whipple expression. 2017

	d_{max}	E_{max} [eV]	Voltage [V]
default	2.4982	316.23	$-10.5 \cdot 10^{3}$
$d_{max} + 10\%$	2.7481	316.23	$-10.3 \cdot 10^{3}$
$d_{max} - 10\%$	2.4897	316.23	$-10.6 \cdot 10^{3}$
$E_{max} + 10\%$	2.4982	347.85	$-10.3 \cdot 10^{3}$
$E_{max} - 10\%$	2.4982	284.61	$-10.6 \cdot 10^{3}$

Table 3.7: Results of variation in the isotropic Sims expression. 2017

what SEE model is more accurate but to illustrate the importance of the choice of SEE model. Considering that Katz and Sims model are more complex models that Whipple one, and they fit well at high energies, it could be suggested that one of this would be desirable to be more accurate. However, it is not possible without experimental data to make a clear statement about this.

3.2.4 Variation in SEE for normal particle incidence

Since the input values are required to be introduced as normal particle incidence, it would be interesting to evaluate the SEE variation for this kind of particle incidence. In this case, it was analyzed for three different models by Wrenn and Sims (Katz, Whipple and Sternglass). However, The Sternglass model is not currently available therefore the study was performed with the same models used in the previous section. Figure 3.9a shows the SEE curves presented in 1989, meanwhile figure 3.9bshows the respective curves obtained in 2017. The curves are pretty similar between models and between analysis. In normal incidence, it is possible to see that the peaks are coincident and they act like isotropic case: Katz et Whipple coincides at low energies while at high energies Whipple model obtains a higher yield and Sims and Katz are nearly equal.

The effects in equilibrium potential when varying the value of the peak and its position can be seen at table 3.8. Regarding Katz and Sims models, this variation remains relative insensitive to changes. For Whipple model, the effects are more noticeable (between 4% and 10%). In contrast to isotropic incidence, the variation of potential between models is lower.

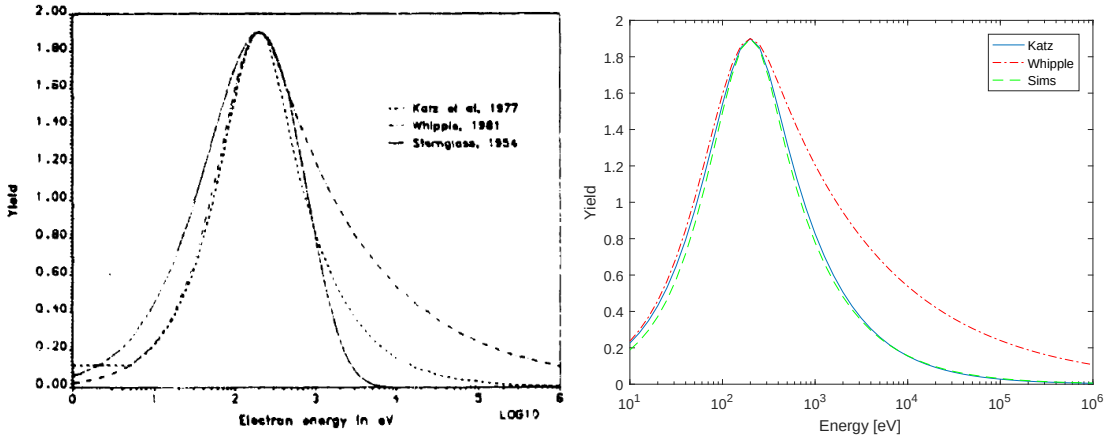

(a) SEE curves from the 1989 analysis [14]

(b) SEE curves from the 2017 analysis

Figure 3.9: Secondary electrons yield for Kapton; normal particle incidende

	d_{max}	E_{max} [eV]	Katz Voltage [V]	Whipple Voltage [V]	Sims Voltage [V]
default	1.90	200	$-16.5 \cdot 10^3$	$-12.8 \cdot 10^3$	$-16.5 \cdot 10^3$
$d_{max} + 10\%$	2.09	200	$-16.4 \cdot 10^3$	$-12.2 \cdot 10^3$	$-16.4 \cdot 10^3$
$d_{max} - 10\%$	1.71	200	$-16.6 \cdot 10^3$	$-13.3 \cdot 10^3$	$-16.6 \cdot 10^3$
$E_{max} + 10\%$	1.9	220	$-16.5 \cdot 10^3$	$-12.6 \cdot 10^3$	$-16.4 \cdot 10^3$
$E_{max} - 10\%$	1.9	180	$-16.6 \cdot 10^3$	$-13.0 \cdot 10^3$	$-16.5 \cdot 10^3$

Table 3.8: Results of varying the normal SEE function

3.2.5 Changes in the current of backscattered electrons

The backscattered electron current is calculated by Equipot using an expression described by Whipple, as commented in chapter 2. Two parameters affect this current: the atomic number and the incidence of the electron particles. This last parameter is included in the study of SEE previously presented. Therefore, the only parameter that may be varied in order to investigate changes in energy is the atomic number. Table 3.9 shows the result of this variation. As it is shown, the effect of varying the atomic number is negligible.

	$AtomicNumber(Z)$	Voltage [V]
default	5	$-10.5 \cdot 10^3$
$d_{max} + 10\%$	5.5	$-10.5 \cdot 10^3$
$d_{max} - 10\%$	4.5	$-10.6 \cdot 10^3$

Table 3.9: Results of small changes in atomic number. 2017

3.2.6 Changes in the secondary electron current due to ion impact

This current component is defined by two parameters: the yield for incident 1keV protons and the energy at the maximum yield. Table 3.10 shows the results of changing these parameters by a 10%. As it possible to see, the variation in equilibrium potential are lower than 10% (about 5%). This result coincides with that expected following the previous study.

	Yield (1 keV)	E_{max} [keV]	Voltage [V]
default	0.455	140	$-10.5 \cdot 10^3$
$Y_{max} + 10\%$	0.501	140	$-10.0 \cdot 10^3$
$Y_{max} - 10\%$	0.410	140	$-11.1 \cdot 10^3$
$E_{max} + 10\%$	0.455	154	$-10.4 \cdot 10^3$
$E_{max} - 10\%$	0.455	126	$-10.7 \cdot 10^3$

Table 3.10: Effects of vaying SEE due to ion impact. 2017

3.2.7 Analysis of different materials at the same environment

It was thought that it would be interesting to present how the equilibrium potential varies when changing the patch material used. Equipot code has a large option of materials from which a selection of 5 materials have been used in the analysis. The properties of each materials are shown in table 3.11.

	Kapton	Indium tin oxide coating	Teflon	Epoxy Resin on Conducting Carbon Fibre	Oxydized Aluminium	Gold
Thickness [m]	$2.50 \cdot 10^{-5}$	0.001	2.50·10−5	$2.00 \cdot 10^{-6}$	$1.00 \cdot 10^{-3}$	$1.00 \cdot 10^{-2}$
Relative Permittivity	3	3	2	3.5	9	3
Conductivity [ohm/m]	$1.0 \cdot 10^{-15}$	$1.00 \cdot 10^{-15}$	$1.00 \cdot 10^{-15}$	$1.00 \cdot 10^{-14}$	$1.00 \cdot 10^{-12}$	$1.00 \cdot 10^{-15}$
Atomic number	5	22	7	10	13	79
Max Normal SEE Yield	1.9	2.5	2.5	1.6	3.2	1.3
Energy at Max Normal SEE Yield [keV]	0.2	0.3	0.25	0.35	0.35	0.8
Yield of 1 keV Protons	0.455	0.49	0.455	0.455	0.244	0.413
Energy at Max Proton Yield [keV]	140	123	140	140	230	135
Photoelectron yield $[Am^{-2}]$	$2.00 \cdot 10^{-5}$	$3.20 \cdot 10^{-5}$	$2.00 \cdot 10^{-5}$	$2.05 \cdot 10^{-5}$	$4.00 \cdot 10^{-05}$	$2.90 \cdot 10^{-5}$

Table 3.11: Characteristics of Materials

As in the previous analysis, it was selected the SCATHA environment as it is considered the worst one. In figure 3.10, it is possible to see a bar diagram where the different materials are compared. In order to make possible a graphical comparison, it has been used a logarithmic scale and the values of the equilibrium potential correspond to the absolute values one to make possible to use this scale. To be precise, indium and gold are charged with a positive potential meanwhile the other materials have negative equilibrium potentials. Following the Standard ECSS-E-ST-20-06C, the maximum potential that a material must withstand is about 1 keV. Checking the cited figure, neither Kapton nor Teflon fulfill this condition. If we have a satellite made of these materials, in an environment like that of SCATHA conditions would withstand the equilibrium potential and would led to damage in the structure. By other side, indium and gold have equilibrium potentials

near to the nullity. In terms of spacecraft charging, the two materials would be the best ones because even in the worst conditions, they have quite low potential. Nevertheless, due to their high density, they are not very used materials because the cost of their weight is not compensated by the low capacity of charging.

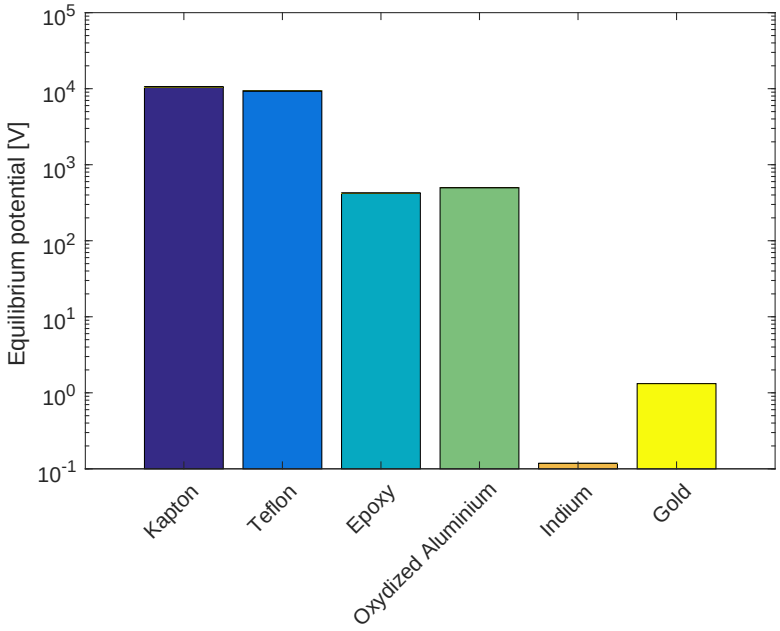

Figure 3.10: Comparison of equilibrium potential of different materials at SCATHA environment

3.2.8 Analysis of one material at different environments

At the beginning of this chapter, the different environments available at Equipot code are stated at table 3.1. In this subsection, the idea is to compare the performance of a material placed at different environments. To provide a useful design in terms of spacecraft charging, it is desirable to select the material whose variation in equilibrium potential among environments is the lowest. The materials used in this analysis are those used in the previous one with the same characteristic parameters.

Since the difference between materials is quite important, it is not possible to show all the materials in a unique figure. Therefore, the analysis has been divided by materials and each material has one graphical representation for environments at low altitude and at high altitude. The values represented in the graph for each material at each environment can be looked up at table 3.12.

Results for the case of the ColdMaxwellians for ram test are the same for several materials. This ambient produces a floating potential. The ion current depends here on the ion ram velocity, i.e. the velocity of spacecraft in LEO, $V_s \approx 7.7$ km/s. The electron current depends on $\exp\left[eV/\left(k_B T_e\right)\right]$ and the electron thermal velocity, which is $v_{te} \approx 1.32 \cdot 10^3$ km/s for $T_e = 0.1$ eV. The floating potential for vanishing net current reads

$$V = -\frac{K_B T_e}{e} \log\left(\frac{V_s}{v_{te}}\right), \tag{3.1}$$

which is about -0.514 V with the parameters considered.

The figures have logarithmic scale and absolute value to make possible the comparison in terms of magnitude of potential. Since the risks for spacecraft do occur if the absolute value of equilibrium potential is higher than 1 kV, the sign of the charge in this consideration can be negligible in this case.

Following the found results, is interesting to see that many of the materials that in SCATHA environment conditions are not suitable for a space mission, have low potentials at other environments. It is in this case when it should be considered the time of charging of the material. If those material having high potential need large times to obtain this potential, it would be possible to implement active mitigation techniques that prevent this effect. For example, in SCATHA environment, Kapton material needs $2.58 \cdot 10^6$ ms to reach equilibrium potential. That means that this material would be charged with $10.5 \cdot 10^3$ eV in 43 minutes. The selection of the material should be a compromised among how good is it in terms of spacecraft charging, the economic cost of this material, its mass density to avoid high weight for the spacecraft, and the capability of mitigating the spacecraft charging effects. One good option could be the oxidized aluminium. The values of equilibrium potential are higher than gold and indium ones. However, the charging time is high enough to prevent spacecraft charging effects.

	Environment	Kapton	Indium tin oxide coating	Teflon	Epoxy Resin on Conducting Carbon Fibre	Oxydized Aluminium	Gold
High Altirude	SCATHA	$-1.05 \cdot 10^4$	$1.18 \cdot 10^{-1}$	$-9.39 \cdot 10^3$	$-4.22 \cdot 10^2$	$-5.00 \cdot 10^2$	1.32
	NASA WORST CONDITIONS (NWC)	$-7.29 \cdot 10^3$	$9.36 \cdot 10^{-1}$	$-6.46 \cdot 10^3$	$-5.32 \cdot 10^2$	$7.06 \cdot 10^{-1}$	2.27
	METEOSAT QUIET (MQ)	2.41	5.37	3.45	5.51	6.03	4.78
	METEOSAT DISTURBED (MD)	2.64	4.84	2.05	1.90	4.95	6.16
	NASA AVERAGE GEO (NAG)	1.14	5.09	2.46	2.41	5.12	6.32
Low Altirude	IRI SOLAR MIN -WINTER (ISMW)	$-5.21 \cdot 10^{-1}$	$-1.97 \cdot 10^{-1}$	$-3.66 \cdot 10^{-1}$	$-3.98 \cdot 10^{-1}$	$-1.67 \cdot 10^{-1}$	$-2.56 \cdot 10^{-1}$
	IRI SOLAR MAX - SUMMER (ISMS)	$-7.25 \cdot 10^{-1}$	$-6.32 \cdot 10^{-1}$	$-6.92 \cdot 10^{-1}$	$-6.99 \cdot 10^{-1}$	$-6.10 \cdot 10^{-1}$	$-6.58 \cdot 10^{-1}$
	COLD MAXWELLIANS RAM (CMR)	$-5.14 \cdot 10^{-1}$	$-5.14 \cdot 10^{-1}$	$-5.14 \cdot 10^{-1}$	$-5.14 \cdot 10^{-1}$	$-5.14 \cdot 10^{-1}$	$-5.14 \cdot 10^{-1}$
	AURORAL TYPE SPECTRA (ATS)	$-2.24 \cdot 10^3$	-1.55	$-1.14 \cdot 10^3$	$-9.10 \cdot 10^2$	-1.55	-1.48
	TEST SPECTRA MAXWELLIANS (TSM)	-1.96	-1.89	-2.19	-2.16	-1.88	-1.86
	COLD MAXWELLIANS FONTHEIM (CMF)	$-2.74 \cdot 10^4$	$-2.96 \cdot 10^3$	$-2.49 \cdot 10^4$	$-4.57 \cdot 10^3$	$-3.69 \cdot 10^3$	$-5.20 \cdot 10^1$
	MAXWELLIAN 1000 KMS + AURORA (MA)	$-7.06 \cdot 10^{-1}$	$-5.58 \cdot 10^{-1}$	$-7.84 \cdot 10^{-1}$	$-8.31 \cdot 10^{-1}$	$-5.01 \cdot 10^1$	$-6.32 \cdot 10^1$

Table 3.12: Equilibrium Potential [eV] for different materials at different environments

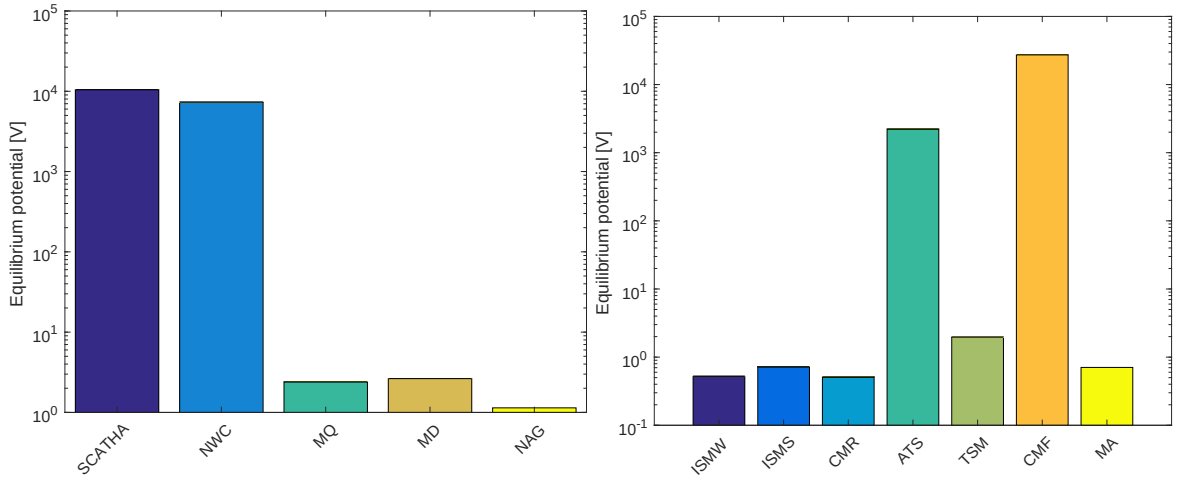

(a) High altitude environments

(b) Low altitude environments

Figure 3.11: Comparison of equilibrium potential at different environment for Kapton

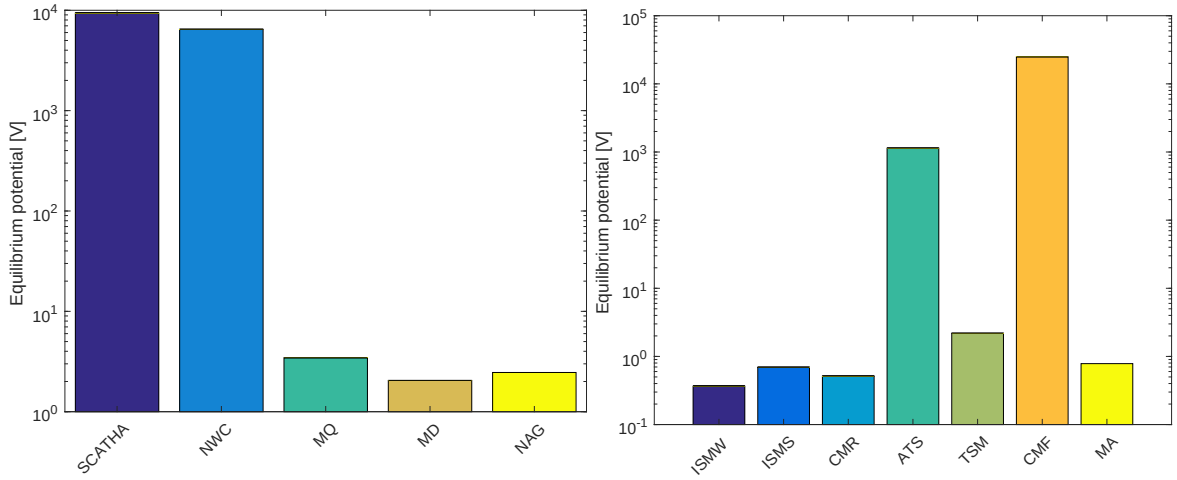

(a) High altitude environments (b) Low altitude environments

Figure 3.12: Comparison of equilibrium potential at different environment for Teflon

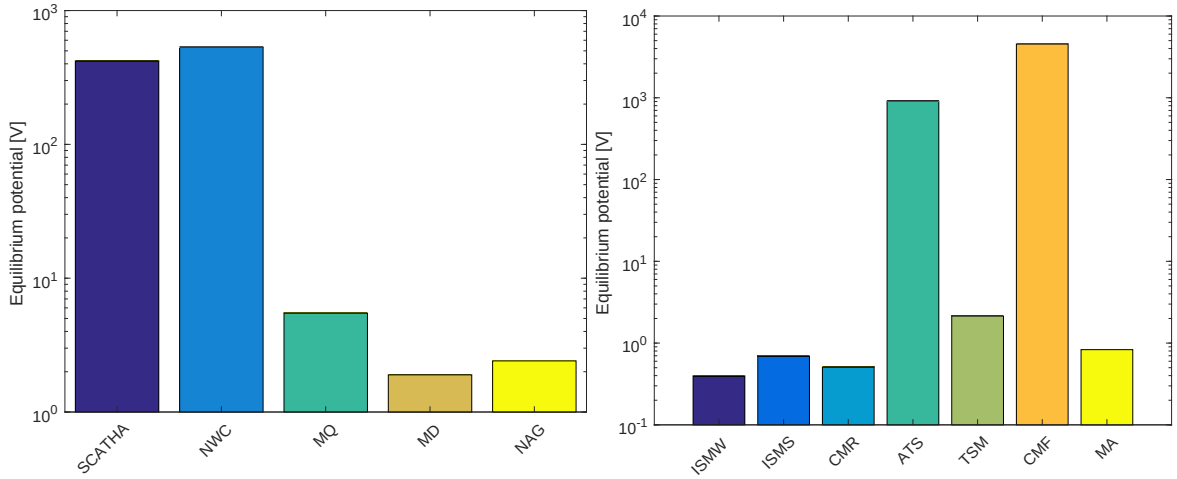

(a) High altitude environments (b) Low altitude environments

Figure 3.13: Comparison of equilibrium potential at different environment for Epoxy resin on conducting carbon fibre

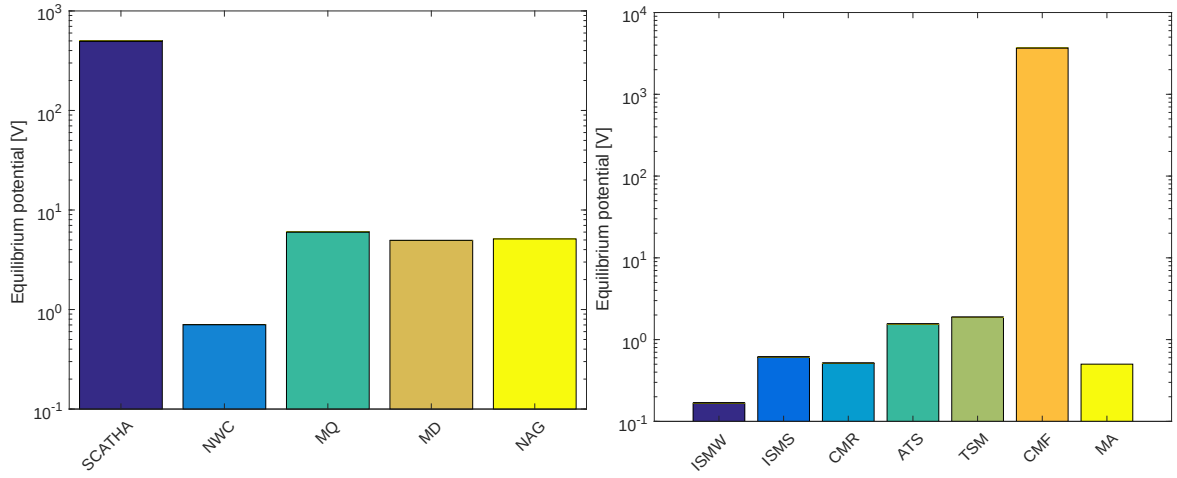

(a) High altitude environments (b) Low altitude environments

Figure 3.14: Comparison of equilibrium potential at different environment for Oxydized Aluminium

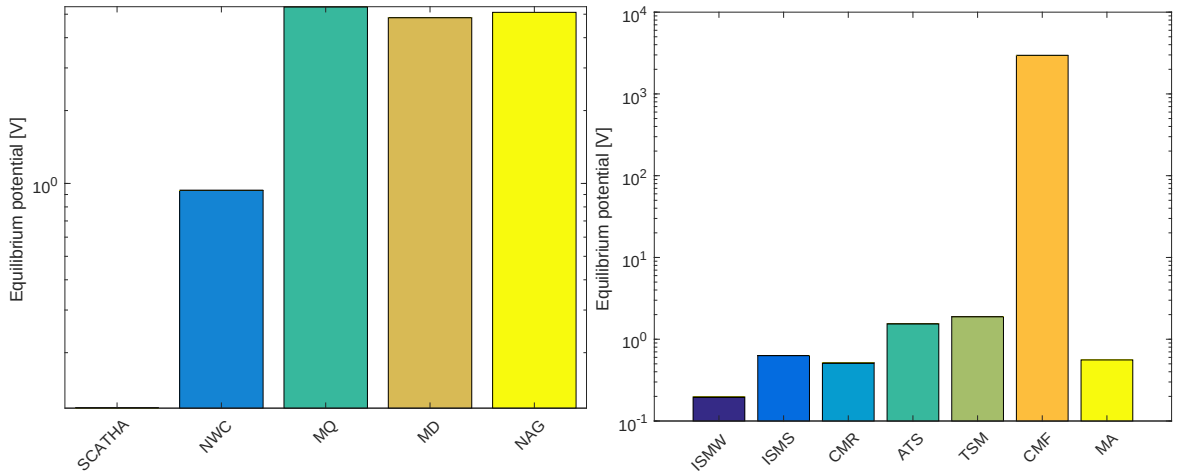

(a) High altitude environments (b) Low altitude environments

Figure 3.15: Comparison of equilibrium potential at different environment for Indium tin oxide coating

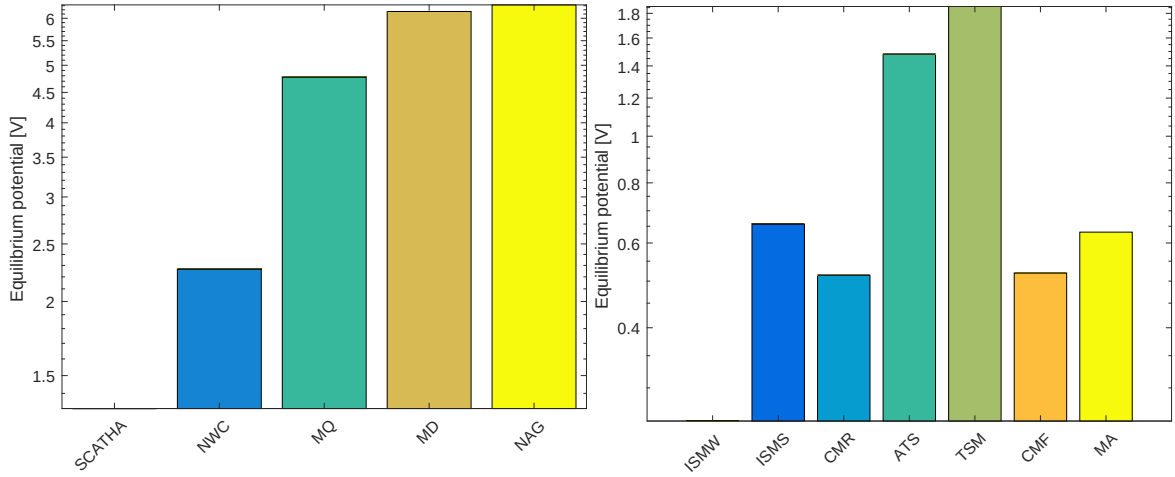

(a) High altitude environments (b) Low altitude environments

Figure 3.16: Comparison of equilibrium potential at different environment for Gold

3.2.9 Analysis conclusion

It has been demonstrated that Equipot is a useful code for spacecraft charging analysis. It is a very user-friendly tool and it is not necessary any training to used it. Lots of parameters can be varied and many combinations of situations are offered. Although the results may not be presented in a fancy form, the calculations are fast and the analysis can be performed in brief time.

This tool has two important limitations. The first one is the geometry of the body to be studied. In contrast with other codes, Equipot perform a 3D analysis with a fixed geometry and does not offer the possibility of implementing a new geometry. This makes the result as not accurate as needed. Due to all of this, this tool can only be used as a first assessment in the design procedure.

The second limitation of this code is that the calculations are limited at Earth's environments. Nowadays, the space missions are oriented along all the Solar System. Planets such Jupiter and Saturn have magnetospheres greater than Earth's one. Therefore, the implementation of environments at other planets in this tool should be interesting. In the following chapter, an approach of this code at Jupiter and Saturn magnetosphere will be presented.

Chapter 4

Spacecraft Charging at Jupiter and Saturn

Surface charging at GEO is the best-known plasma interaction at Earth. However, this effect is not just a concern for spacecraft at Earth, but also throughout the solar system. In particular, elevated levels of charging are also expected at Jupiter and Saturn.

The code used in the previous chapter, Equipot, only works for Earth environments. Within the SPENVIS models, Jupiter environments are being implemented; but Equipot tool still has not available this option. In this chapter, it is going to be presented a possible approach of this implementation. This work was based on "Comparison of Spacecraft Charging Environments at Earth, Jupiter, and Saturn" written by Garrets and Hoffman in 2000 [51].

Figure 4.1: Jupiter planet Credit: NASA. Juno mission

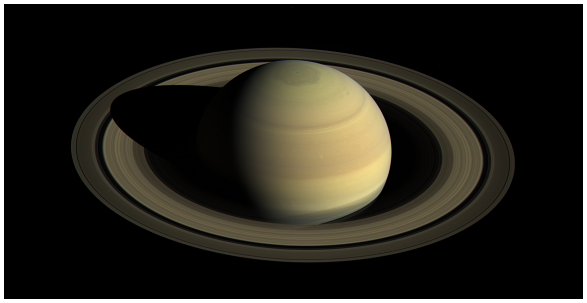

Figure 4.2: Saturn planet Credit: NASA. Cassini mission

	Earth	Jupiter	Saturn
Equatorial radius [km]	$6.38 \cdot 10^3$	$7.14 \cdot 10^4$	$6 \cdot 10^4$
Magnetic Moment [$G - cm^3$]	$8.1 \cdot 10^{25}$	$1.59 \cdot^{30}$	$4.30 \cdot 10^{28}$
Rotation Period [h]	24	10	10.23
Aphelion/Perihelion(au)	1.01/0.98	5.45/4.95	10.06/9.01

Table 4.1: The planets' magnetospheres [51]

4.1 Magnetosphere

In the Introduction chapter of this bachelor thesis, it has been presented the Earth's magnetosphere. As commented, the magnetosphere is an area of space around a planet controlled by the magnetic field of that planet.

The characteristics values for Earth, Jupiter and Saturn's magnetosphere can be seen at table 4.1. The magnetic field at equator is proportional to the magnetic moment divided by the cube of the radial distance. Due to this relation, the Earth and Saturn magnetospheres have similar scale relative to their planetary radii. However, Jupiter has a strong magnetic field that makes its magnetosphere estimated to be 100 times larger.

4.1.1 Jupiter's Magnetosphere

Jupiter has known to have a magnetosphere since 1960. In 1983, it was proposed the Divine-Garrett model [52] that characterized the jovian magnetosphere. In the development of this model, it was incorporated in situ measurements of the Pioneer and Voyager spacecraft, earth-bases observations, and concepts advanced from already presented theoretical models.

Jupiter's Magnetosphere stands 100 times the radius of the planet, being the biggest magnetic field of the Solar System after the sun. This magnetic field is created by a core of compressed liquid metal hydrogen. The jovian moon Io has intense volcanic activity that ejects particles into Jupiter's magnetospheres at 5.9 times the radius of the Jupiter. These particles create radiation belts and the large auroras. The Hubble telescope have registered recently polar auroras from Jupiter as it can be seen in figure 4.4 . The rapid rotation of Jupiter (about 10 h) forces the cold plasma trapped in the magnetosphere to co-rotate at high velocities. These particles form a torus around the planet as it can be seen in figure 4.3 [1]. That would produce new current elements that appear in the equilibrium equation. The magnetic field tilt relative to its spin axis is also dominant in this magnetosphere. The combination of this tilt angle and rotation rate cause that at a given location plasma parameters very radically during a 10h period.

It is important to remark the size of this magnetosphere, being near 15 times the radius of the Sun. Jupiter is placed at 5 astronomical units (au), therefore the photoelectron flux is about 25 times less than at the Earth, becoming a less dominant component that in our planet.

[1] Obtained from School of astronomy and space science, Nanjing University at http://astronomy.nju.edu.cn/ lixd/GA/AT4/AT411/HTML/AT41104.htm

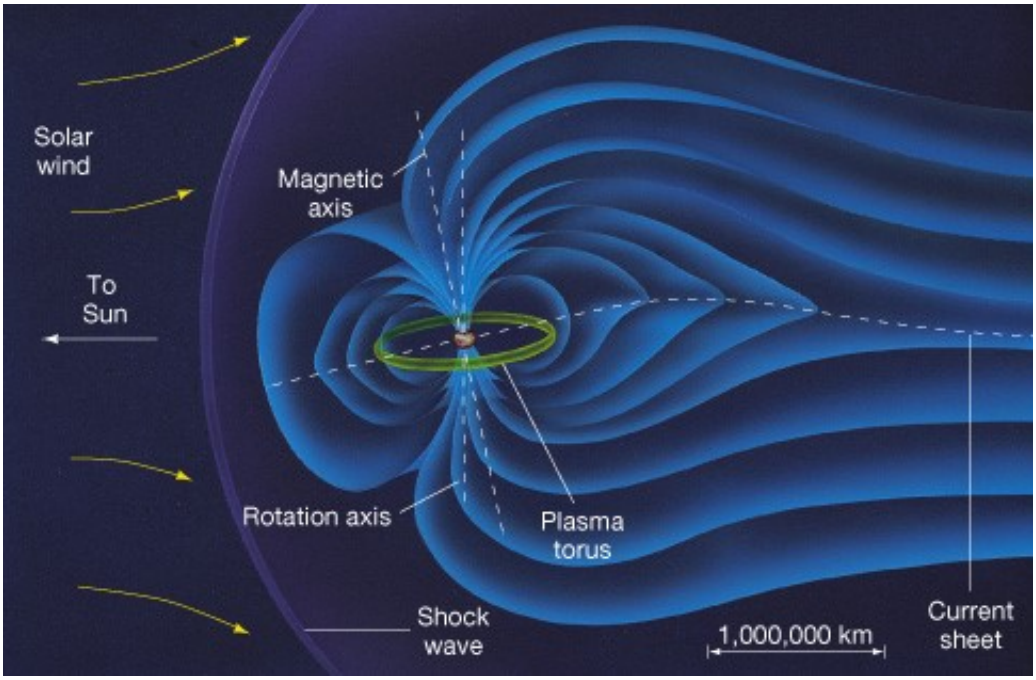

Figure 4.3: Jupiter's magnetosphere

Following the paper written by Garrett et al. [51], the jovian environment can be split in three populations: cold plasma associated with the Io torus, the intermediate plasma and the radiation environment.

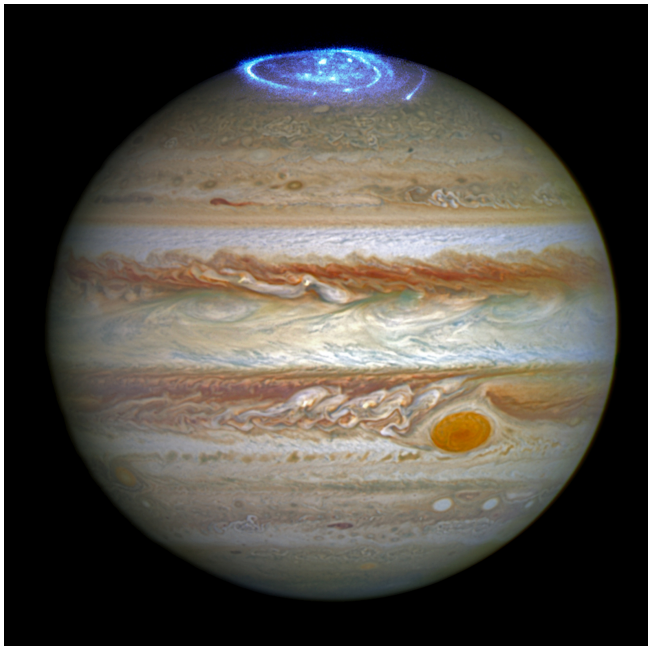

Figure 4.4: Jupiter planet. Note that aurora phenomena can be seen in the north polar cap. Credit: NASA. Hubble

Juno mission entered in Jupiter's orbit in July 2016. Among other measurements, this mis-

sion will study the magnetic field of Jupiter. Juno will offer a new vision and the increment of information that it will be recollected will lead us to a better understanding of the planet and its surroundings.

4.1.2 Saturn's Magnetosphere

In contrast to Jupiter, Saturn Magnetosphere has barely been studied. The most information that we had until Cassini mission were the obtained through brief encounters of the Pioneer 11 and the two Voyager spacecraft. Since 2004, when Cassini mission arrives to the orbit of Saturn, this spacecraft have made some research about this topic. It has mapped the magnetic field, studying the flow of gases and how it affects to Saturn's auroras.

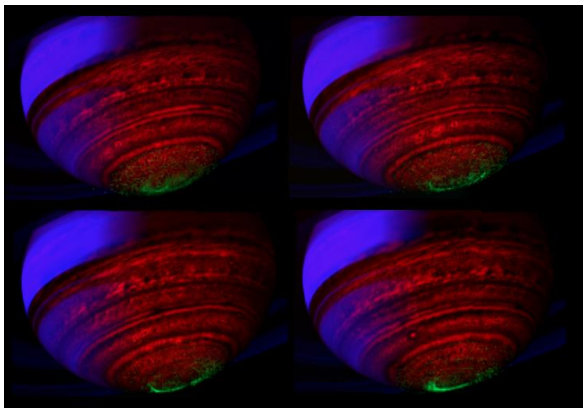

Figure 4.5: Saturn's aurora observed by Cassini spacecraft. Credit: NASA. Cassini mission

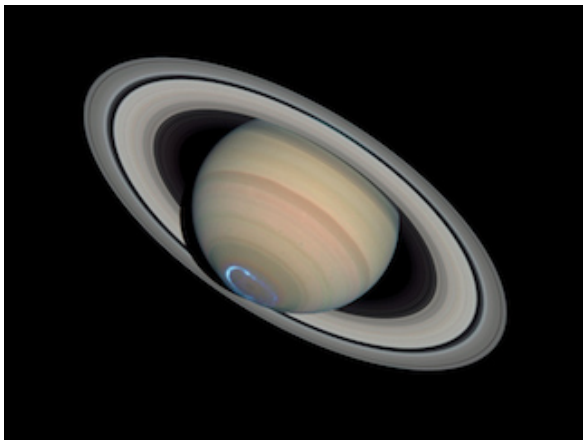

Figure 4.6: Saturn's aurora observed by Hubble telescope. Credit: NASA. Hubble

It was known that the Saturn's magnetic field were aligned with its axis of spin, so the plasma ring around Saturn is relatively steady compared to that of Jupiter. As in the other planet, the magnetic field of Saturn is influenced for one of its moons, Titan. Although it is not inside the magnetosphere like Io at Jupiter's one, it contributes a large cloud of neutral gas in the outer magnetosphere. By other side, Saturn's ring E is fed by material blasted into space by another moon, Enceladus. This material is a major source of plasma fueling Saturn's magnetosphere.

Saturn's magnetosphere appears to be intermediate in nature to those of Earth and Jupiter. Similar to Jupiter, the photoelectron flux is lower than at the Earth (about 100 times lower). However, the photoelectron flux is a dominant component at night and at the outer magnetosphere.

In addition to the already mentioned components, the dust has a significant role within the magnetosphere. The impact of the rings and the dust within the Saturn's magnetosphere is one of the point of research about this topic. Cassini spacecraft provided a lot of information about the planet and its satellites during the 20 year-long mission. Many of the expected values were obtained but there were remarkable differences with respect to other measurements made before. Cassini discovered the influence of Enceladus in the ring E and the magnetosphere. It tried to measure the period of Saturn but the results obtained were not coincident with those obtained with Voyager spacecraft. The period measured by Cassini were lower than period measured by Voyager and even this data was varied since Cassini had arrived at Saturn.

The report on which is based the calculations of this bachelor thesis was proposed 4 years before the arrival of Cassini at Saturn so it is possible that the values used would not be coincident with values measured recently. However, they are accurate enough to make a possible estimation of potential measurements at Saturn's orbit. It would be advisable to make an update of the data when the Cassini results would be published.

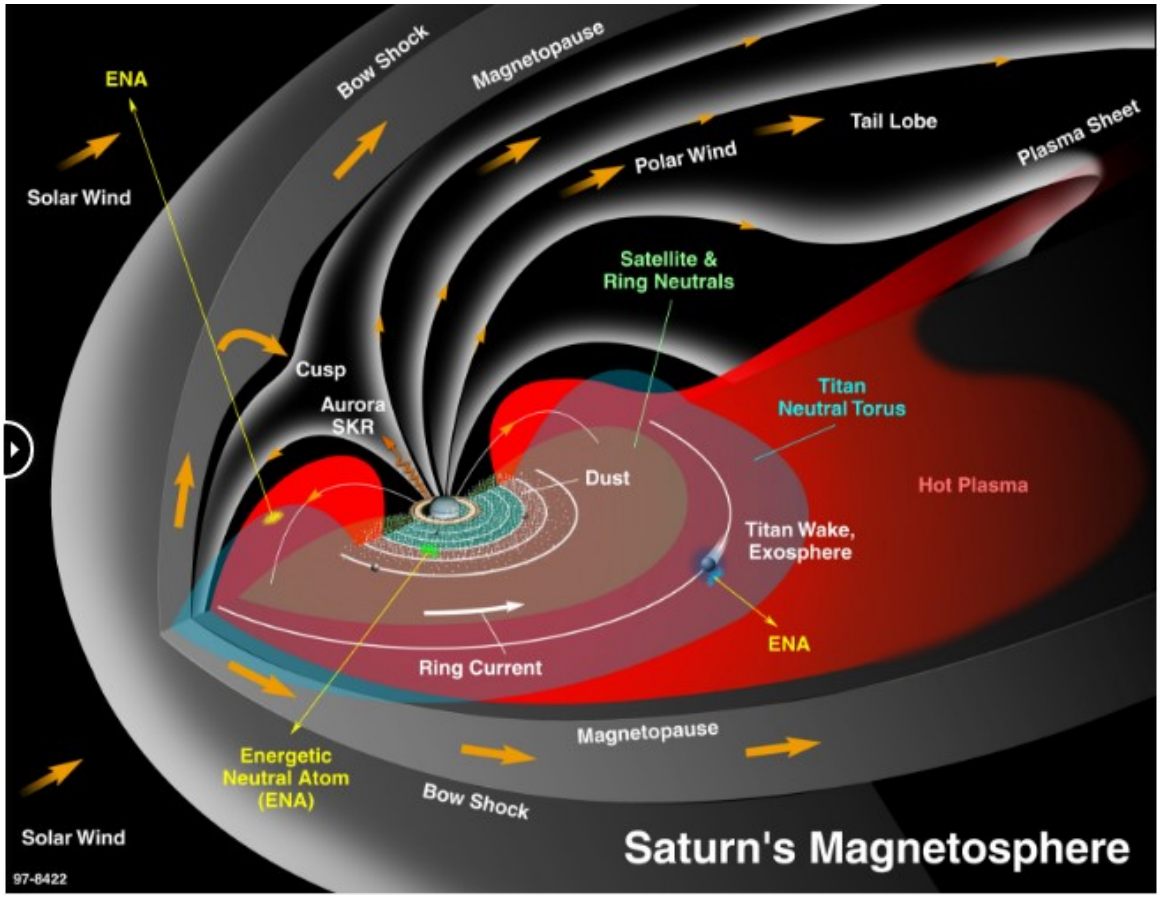

Figure 4.7: Saturn's magnetosphere. Credit: NASA

4.2 Energy Distribution Functions

In previous section, it has been mentioned different energy distribution functions when talking about the environments implemented in the Equipot tool. Prior to the theoretic analysis of Jupiter and Saturn's magnetosphere, the different energy distribution functions will be presented. A distribution function is the mathematical description of a statistical approach used to characterize the velocity that may have an individual particle.

4.2.1 Maxwellian Distribution

In thermal distribution, the Maxwellian distribution function in terms of scalar velocity is described by:

$$f(v) = 4\pi n \left(\frac{m}{2\pi K_B T}\right)^{\frac{3}{2}} v^2 e^{\left(-\frac{v^2 m}{2KT}\right)} \tag{4.1}$$

where n is the density, K is the Boltzmann constant, v is the scalar velocity and T is the temperature.

A pair of numbers for density and temperature is needed to describe the complete distribution.

4.2.2 Double Maxwellian Distribution

There exist unstable velocity distributions that are non-Maxwellian distributions with some sort of anisotropy, for example a beam. Both plasmas are Maxwellian independently. However, the combination of both plasma is a double Maxwellian distribution function, which is described by two pairs of numbers for density and temperature. Being a hot and a cold plasma, the distribution function is

$$f(v) = 4\pi n_h \left(\frac{m_h}{2\pi K_B T_h}\right)^{\frac{3}{2}} v^2 e^{\left(-\frac{v^2 m_h}{2K_B T_h}\right)} + 4\pi n_c \left(\frac{m_c}{2\pi K_B T_c}\right)^{\frac{3}{2}} v^2 e^{\left(-\frac{v^2 m_c}{2K_B T_c}\right)} \tag{4.2}$$

This distribution was the most used in this bachelor thesis, being the velocity distribution function used in SCATHA worst environment.

4.2.3 Bi-Maxwellian Distribution

There exit unstable velocity distributions with a temperature anisotropy. This means that the temperature characterizing the movement of the particle is different depending on the particle direction. A two-dimensional distribution must be used. It is considered a stable 2D distribution when there is a Maxwellian distribution in both the parallel and perpendicular direction. This distribution is independent from the direction.

$$f(v_\perp, v_\parallel) = 2\pi n \frac{m\sqrt{m}}{\sqrt{\pi^3 2K_B T_\parallel} 2K_B T_\perp} v_\perp e^{-\left(\frac{v_\perp^2 m}{2K_B T_\perp} + \frac{v_\parallel^2 m}{2K_B T_\parallel}\right)} \tag{4.3}$$

4.2.4 Kappa Distribution

Previous distributions are adequate for many purposes. Nevertheless, they do not join smoothly onto the high energy spectra for electrons and protons. The Kappa distribution was employed to derive a distribution that fits better for higher energies. Kappa distribution function was shown for the first time by Vasyliunas [53]. This distribution functions have high-energy tails deviating from

Maxwellian and decreasing as power law in particle speed [54]:

$$f(v) = \frac{n}{2\pi(\kappa\omega^2)^{3/2}} \frac{\Gamma(\kappa+1)}{\Gamma(\kappa-1/2)\Gamma(3/2)} \left(1 + \frac{v^2}{\kappa\omega^2}\right)^{-(\kappa+1)} \tag{4.4}$$

where $\omega = \sqrt{(2\kappa-3)K_B T/\kappa}$ is the thermal velocity, m the mass of the particles, n their number density, T their equivalent temperature, v the velocity of the particles and $\Gamma(x)$ is the Gamma function. The value of κ determines the slope of the energy spectrum. As it is represented in figure 4.8, in the limit $\kappa \to \infty$ the Kappa function becomes a Maxwellian distribution.

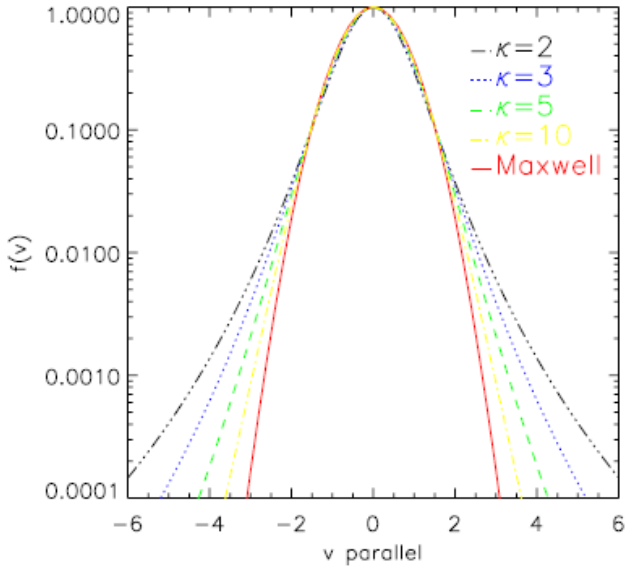

Figure 4.8: The Kappa velocity-distribution function for different values of the κ parameter. [54]

4.3 Implementation of charging code for Jupiter and Saturn

The charging code at Jupiter and Saturn magnetosphere was developed following the algorithm used in the Equipot tool. The code was implemented in MATLAB software. The idea is to find a value of the potential that makes the equation 2.1 equals to zero. Following this idea, each current component is calculated for an initial potential value and then it was used the MATLAB function called $fzero$ to obtain the value of the potential that fulfilled the condition. As it was explained before, the magnetosphere of Jupiter and Saturn is different from Earth one. Due to this reason, the equation 2.1 should be adapted to the desired magnetosphere. It was followed the procedure presented by Garrett and Hoffman [51].

In this implementation, the secondary and backscatter surface currents had been parametrized by fitting them in terms of the temperature, number density, and potential. The material chosen is aluminium because it is a common used spacecraft material. The photoelectron current is also parameterized in terms of the potential and material. Therefore, the focus of this implementation was the electron, proton and ion current. Representative values for the plasma regions at Jupiter, and Saturn are presented in Table 4.2 [51]. The values used in the code for the calculations were taken from this table.

Region	J_{ph}	n_{e1}	E_{e1}	n_{e2}	E_{e2}	n_{ek}	E_{ek}	κ_e	n_{hk}	E_{hk}	κ_p	V_s	n_{pc}	E_{pc}	A_m	n_{ic}	E_{ic}
Jupiter																	
Cold Torus 3.5 Rj	0.08	50	0.5	-	-	5	1000	2.1	1	30000	2.0	44	-	-	32	50	0.5
Warm Torus 5.5 Rj	0.08	1000	1	-	-	10	1000	2.0	1	30000	3.0	69	-	-	24	1000	2
Hot Torus 7 Rj	0.08	1000	10	-	-	5	500	2.0	5	50000	4.2	85	-	-	24	1000	40
Plasmasheet 8 Rj	0.08	12	50	-	-	2	500	2.0	5	40000	3.5	100	-	-	16	12	50
Saturn																	
Inner plasma-sheet 4-8 Rs	0.02	2.15	20	-	-	0.196	262	1.8	0.005	29833	7.4	40	3.2	15	16	30.15	73
Extended Plasma-sheet 8-12 Rs	0.2	0.7	28	-	-	0.111	458	1.7	0.003	30800	8.5	8.0	0.74	26	16	2.5	246

Table 4.2: Representative values of the charging environment at Jupiter and Saturn. [51]

To account for all the current present at Jupiter and Saturn, the equation 2.1 was expanded to include Maxwellian and Kappa distribution components together with a heavy ion component. This last term can be selected to be treated as corotating or Maxwellian component. The code was performed twice, varying this last component in order to see the difference and select which one is more appropriate for each population.

Maxwellian components where obtained using equations 2.6 and 2.7. Regarding Kappa distribution components, they were calculated using the following expressions

$$I_{e\kappa} = AJ_{e\kappa 0}\left(1+\frac{|V|}{\kappa_e E_{ek}}\right)^{(\kappa_e-1)}; \tag{4.5}$$

$$I_{i\kappa} = AJ_{e\kappa 0}\left(1+\left(\frac{\kappa_i-1}{\kappa_i}\right)\frac{|V|}{E_{i\kappa}}\right); \tag{4.6}$$

where

A area of the body

V potential

E_κ characteristic energy for Kappa distribution

$J_{\kappa 0}$ ambient current for Kappa distribution

The ambient current for Kappa distribution is then obtained from

$$J_{e\kappa 0} = q_e n_{e\kappa} \sqrt{\frac{2E_{ek}\kappa_e}{m_e \pi}} \frac{2\Gamma(\kappa_e - 1)}{\Gamma(\kappa_e - 1/2)}; \tag{4.7}$$

where q is the charge of the particle, n its density, E its characteristic energy, and m the particle mass. Subindex "e" refers to "electron"; subindex "i" reffers to "ion". As a remainder from the previous chapter, in order to obtain potential in eV, the factor of conversion previously mentioned should be applied here.

For co-rotation plasma, the ion current is given by the expression given below:

$$I_R = q_p \pi R^2 n_i V_s \tag{4.8}$$

where R is the radius of spherical spacecraft, considered to be 1 meter as used in the Equipot tool, n_i is the heavy ion density and V_s is the spacecraft velocity relative to plasma. As mentioned, the values of the component for the various plasma regions are listed in Table 4.2 where

J_{ph} photoelectron current $[nA/cm^-2]$;

n_{e1} electron cold component density $[cm^-3]$;

E_{e1} electron cold component characteristic energy $[eV]$;

n_{e2} electron hot component density $[cm^-3]$;

E_{e2} electron hot component characteristic energy $[eV]$;

n_{ek} electron Kappa component density $[cm^-3]$;

E_{ek} electron Kappa component characteristic energy $[eV]$;

κ_e electron Kappa value;

n_{hk} proton Kappa component density $[cm^-3]$;

E_{hk} proton Kappa component characteristic energy $[eV]$;

κ_p proton Kappa value;

V_s co-rotation velocity [Km/s];

n_{pc} proton Maxwellian component density $[cm^-3]$;

E_{pc} proton Maxwellian characteristic energy $[eV]$;

A_m atomic nucleon number;

n_{ic} heavy ion density [$cm^{-}3$];

E_{ic} heavy ion Maxwellian characteristic energy [eV];

All the previous parameters were converted to International System prior the calculations Using previous expressions and initial values, two codes for the study of spacecraft charging at Jupiter and Saturn were written: one for the thick sheath assumption for cold ions (heavy ion with Maxwellian distribution) and another for the ram current for cold ions (using equation 4.8 instead of that one used for Maxwellian distribution). There are some regions where there is no population of heavy ions. In these sections, it was used proton Maxwellian component instead, considering the protons as ions of Hydrogen

4.4 Results obtained with the created code

Following the steps of the Garrett and Hoffman's paper, the results obtained from the code implemented in Matlab are shown in table 4.3. In this table, it has been presented the preliminary results from the paper of 2000 and the results obtained following the new code.

Results	Study of 2000		New Study 2017	
	Thick Sheath	Ram Current	Thick Seath	Ram Current
Jupiter				
Cold Torus 3.5 Rj	-459	-37188	-1600.8	-21521
Warm Torus 5.5 Rj	-112	-7315	-468.51	-22588
Hot Torus 7 Rj	-102	-128	-421.23	-1517
Plasmasheet 8 Rj	**-855**	-1316	**-827.26**	-909.46
Saturn				
Inner plasma-sheet 4-8 Rs	-79	-1128	-187.19	-508.2
Extended Plasma-sheet 8-12 Rs	-602	-22832	-288.98	-2.95.86

Table 4.3: Estimate values of potential at different magnetosphere regions.

Although the values have quite difference, in both cases it is possible to conclude that spacecraft charging is not a problem in these environments because most of the values are lower than the maximum admissible potential. It is possible that the low contribution of the photoelectron flux could derive in significant charging. However, this case can be considered an extreme case and only considered for designing purposes.

The difference between codes can be produced for many reasons: the codes used to obtain the potential were different, there is lot of information and it would lead to mistakes and misunderstandings, the iteration process would be different and then getting the potential. The results marked in bold are those value where both codes has similar estimation. It is also possible that Garret et al. implemented a code with data corresponding to all latitude and longitude and used average values. Thus, these data would produce different results.

Chapter 5

Conclusions and Future Work

5.1 Conclusions

The main objectives of this thesis were to present spacecraft charging process, its effects and how it is studied through Equipot tool. Within the introduction chapter, the problem of spacecraft charging was presented and it was demonstrated that is one of the most important hazard in terms of space weather effects. In the following chapters, the physics of this phenomenon has been studied, how spacecraft charging effect changes with the different parameters and an approach to these effects at Jupiter and Saturn environments. The main conclusions derived from the analysis were the following:

- Spacecraft charging is one of the most important hazards to be considered while the design process. Although the spacecraft charging events have decreased in the last years, it still has important impact in the space mission; especially at GEO.

- A simple tool as Equipot can help for preliminary study of spacecraft charging. This tool has many limitations that would not provide a comprehensive analysis of this phenomenon to the design process. For mission where this effect is minimum, a simple analysis like the offered for this code will be enough. In contrast, if the program determines high equilibrium potentials, the design process will need other high-level programs for deeper study. There are tools, which could be used such as Solarc and Dictat that would allow studying particular and specific spacecraft charging issues. There are also very complex tools such as NASCAP that try to take account entire charging effects, increasing the computation time.

- Through the sensitive analysis it was demonstrated that parameters like the angle of incidence of photoelectron flux, the conductivity of the material and the election of SEE model produce important impacts in the charging process.

- The selection of the material is fundamental in the design process. It must be done preliminary studies assessing different materials in order to choose the most appropriate. It is also important to know the environment where the mission take place because some materials can be used at certain environments although they are not a good election for other ones.

- This study can be considered as a prevent method. Sometimes to perform only a prevention study could not be enough for certain missions. Mitigation techniques are needed in those cases. The idea is that the design in terms of spacecraft charging process must be a compromised among net weight, resistance to space weather, safety inside of spacecraft, etc. As an example, an unmanned mission to explore Jupiter like JUNO-type should consider materials that withstand high-energy dose whereas a mission with crew in LEO must have the safety of the astronauts as the main objective.
- Spacecraft charging at Jupiter and Saturn exits and it may be an important concern for missions oriented to the inner magnetosphere. Nevertheless, this phenomenon has lower impact than at Earth's magnetosphere.

5.2 Future Work

Spacecraft charging effects have been reduced since it was being studied. However, there is still a long way regarding this area. This section is dedicated to expose the possible further studies that can be developed.

As it was commented previously, Equipot is a useful tool regarding preliminary analysis at design phase. However, it is limited to Earth's environment. As presented in this project, it would be interesting to expand this code to other planets and moon with magnetosphere or atmosphere.

This thesis has only presented results that were obtained at sunlight conditions. Other advisable studies could be to repeat the sensitive analysis in Equipot code but with eclipse condition and to make comparison between both conditions. In addition to this, the study of the mitigation techniques applied to both condition it is also interesting to be considered.

Regarding the presented results of Jupiter and Saturn's magnetosphere, the values used were out of date. Cassini mission has provided new information about Saturn's magnetosphere that change at all the information we knew about it. Nowadays, Juno mission is at its earliest days and it is expected that it will also find out relevant material about Jupiter magnetosphere. When data from both mission were obtained, it would be interested to update this study to get more realistic results.

Finally, it can be also of interest to perform an analysis of a complete mission in terms of spacecraft charging using the preliminary code presented here. It would consist of studying this phenomenon along the orbit that spacecraft would be using.

It is logical to expect future works to provide solutions to this concern in terms of prevention and mitigation techniques. Our need of exploration will lead us to send new mission further each time and this will lead to the better knowledge of the different magnetosphere along the Solar System and therefore to new theories and techniques to be applied at this area.

Bibliography

[1] "The NESC 2016 technical update," tech. rep., NASA Engineering and Safety Center, 2016.

[2] "The magnetosphere." https://www.nasa.gov/mission_pages/sunearth/overview/Helio-facts.html.
Last accessed 27/08/2017.

[3] H. Koons, J. Mazur, R. Selesnick, J. Blake, J. Fennell, J. Roeder, and P. Anderson, "The impact of the space environment on space systems," in *6th Spacecraft Charging Technology*, pp. 7–11, 1998.

[4] R. D. Leach and M. B. Alexander, "Failures and anomalies attributed to spacecraft charging," 1995.

[5] J. I. Minow and L. N. Parker, "Spacecraft charging: Anomaly and failure mechanisms," 2014.

[6] N. Murdoch, D. Izzo, C. Bombardelli, I. Carnelli, A. Hilgers, and D. Rodgers, "Electrostatic tractor for near earth object deflection," in *59th International Astronautical Congress*, vol. 29, 2008.

[7] E. A. Hogan and H. Schaub, "Impacts of hot space plasma and ion beam emission on electrostatic tractor performance," *IEEE Transactions on Plasma Science*, vol. 43, no. 9, pp. 3115–3129, 2015.

[8] D. Hastings and H. Garrett, *Spacecraft-environment interactions*.
Cambridge university press, 2004.

[9] A. Vampola, "The aerospace environment at high altitudes and its implications for spacecraft charging and communications," *J. Electrostat*, vol. 20, no. 2, 1987.

[10] J. B. Bacon, "Electrostatic discharge issues in international space station program evas," 2009.

[11] S. I. Association *et al.*, "State of the satellite industry report 2017," *Bryce Space and Technology [Available at http://www.sia.org/annual-state-of-the-satellite-industry-reports/2017-sia-state-of-satellite-industry-report/.]*, 2017.

[12] N. Bobrinsky and L. Del Monte, "The space situational awareness program of the european space agency," *Cosmic Research*, vol. 48, no. 5, pp. 392–398, 2010.

[13] PricewaterhouseCoopers(PwC), "A cost-benefit analysis of the SSA programme." Available at http://www.esa.int/About_Us/Business_with_ESA/Space_economy/A_cost-benefit_analysis_of_the_SSA_programme.

[14] A. Sims and G. Wrenn, "Sensitivity analysis with a simple charging code," tech. rep., ROYAL AEROSPACE ESTABLISHMENT FARNBOROUGH (UNITED KINGDOM), 1990.

[15] G. de España, "Disposición 542 del BOE núm. 15 de 2017," *BOE*, vol. 15, p. 4356 a 4382, January 2017.

[16] H. B. Garrett and A. C. Whittlesey, *Guide to mitigating spacecraft charging effects*. John Wiley & Sons, 2012.

[17] "SPENVIS Spacecraft surface charging." `https://www.spenvis.oma.be/htbin/spenvis.exe/SPACECRAFT?%23resetToPrevious(equipot_par.html)`. Accessed: 2017-09-10.

[18] E. C. Whipple, "Potentials of surfaces in space," *Reports on Progress in Physics*, vol. 44, no. 11, p. 1197, 1981.

[19] A. J. Sims, "Electrostatic charging of spacecraft in geosynchronous orbit," tech. rep., DEFENCE RESEARCH AGENCY FARNBOROUGH (UNITED KINGDOM), 1992.

[20] I. Katz, D. Parks, M. Mandell, J. Harvey, D. Brownell Jr, S. Wang, and M. Rotenberg, "A three dimensional dynamic study of electrostatic charging in materials," 1977.

[21] I. Katz, M. Mandell, G. Jongeward, and M. Gussenhoven, "The importance of accurate secondary electron yields in modeling spacecraft charging," *Journal of Geophysical Research: Space Physics*, vol. 91, no. A12, pp. 13739–13744, 1986.

[22] E. Burke, "Secondary emission from polymers," *IEEE Transactions on Nuclear Science*, vol. 27, no. 6, pp. 1759–1764, 1980.

[23] European Cooperation for Space Standardization, Noordwijk, The Netherlands, *Spacecraft Carging*, July 2008.

[24] I. Katz, J. Cassidy, M. Mandell, G. Schnuelle, P. Steen, and J. Roche, "The capabilities of the nasa charging analyzer program," in *Spacecraft Charging Technology-1978*, vol. 2071, p. 101, 1979.

[25] K. Krupnikov, V. Mileev, and L. Nokikov, "A mathematical model of spacecraft charging ('coulomb'tool)," *Radiation measurements*, vol. 26, no. 3, pp. 513–516, 1996.

[26] S. T. Lai, "A critical overview on spacecraft charging mitigation methods," *IEEE Transactions on Plasma Science*, vol. 31, no. 6, pp. 1118–1124, 2003.

[27] I. Katz, D. Parks, S. Wang, and A. Wilson, "Dynamic modeling of spacecraft in a collisionless plasma," 1977.

[28] H. B. Garrett, "The charging of spacecraft surfaces," *Reviews of Geophysics*, vol. 19, no. 4, pp. 577–616, 1981.

[29] I. Langmuir and K. B. Blodgett, "Currents limited by space charge between concentric spheres," *Physical Review*, vol. 24, no. 1, p. 49, 1924.

[30] C. Y. Johnson and E. B. Meadows, "First investigation of ambient positive-ion composition to 219 km by rocket-borne spectrometer," *Journal of Geophysical Research*, vol. 60, no. 2, pp. 193–203, 1955.

[31] V. Krassovsk, "Exploration of the upper atmosphere with the help of the third soviet sputnik," *Proceedings of the IRE*, vol. 47, no. 2, pp. 289–296, 1959.

[32] K. Chopra, "Interactions of rapidly moving bodies in terrestrial atmosphere," *Reviews of Modern Physics*, vol. 33, no. 2, p. 153, 1961.

[33] I. B. Bernstein and I. N. Rabinowitz, "Theory of electrostatic probes in a low-density plasma," *The Physics of Fluids*, vol. 2, no. 2, pp. 112–121, 1959.

[34] A. Davis and I. Harris, "Interaction of a charged satellite with the ionosphere," tech. rep., NATIONAL AERONAUTICS AND SPACE ADMINISTRATION WASHINGTON DC, 1961.

[35] S. F. Singer, *Interactions of space vehicles with an ionized atmosphere*, vol. 18. Pergamon, 1965.

[36] E. C. Whipple Jr, "The equilibrium electric potential of a body in the upper atmosphere and in interplanetary space," 1965.

[37] E. G. Mullen, M. Gussenhoven, and H. B. Garrett, "A'worst case'spacecraft environment as observed by scatha on 24 april 1979.," tech. rep., AIR FORCE GEOPHYSICS LAB HANSCOM AFB MA, 1981.

[38] C. K. Purvis, H. B. Garrett, A. Whittlesey, and N. J. Stevens, "Design guidelines for assessing and controlling spacecraft charging effects," 1984.

[39] M. Standard, "Electromagnetic compatibility requirements for space systems," tech. rep., MIL-STD-1541A (USAF), 30 December, 1987.

[40] H. B. Garrett and A. C. Whittlesey, "Spacecraft charging, an update," *IEEE transactions on plasma science*, vol. 28, no. 6, pp. 2017–2028, 2000.

[41] D. C. Ferguson, "New frontiers in spacecraft charging," *IEEE Transactions on Plasma Science*, vol. 40, no. 2, pp. 139–143, 2012.

[42] D. Rodgers, A. Hilgers, F. Cipriani, and D. Payan, "Overview of european activites," 2016.

[43] D. C. Ferguson and J. I. Minow, "Status of spacecraft charging in the usa," 2016.

[44] D. C. Ferguson, "Nasa std-4005–the leo spacecraft charging design standard," *Paper No. AIAA*, vol. 4035, pp. 26–29, 2006.

[45] M. Ryschkewitsch, "Mitigating in space charging effects-a guideline," *National Aeronautics and Space Administration Technical Handbook (NASA-HDBK-4002A)*, 2011.

[46] D. Ferguson, "Low earth orbit spacecraft charging design handbook," *NASA, Washington, DC, USA, NASA Rep. HDBK-4006*, 2007.

[47] E. Secretariat, "Ecss space engineering-space environment," tech. rep., Technical Report ECSS-E-ST-10-04C, ESA, 2008.

[48] D. Rodgers, A. Hilger, F. Cipriani, J. Mateo-Velez, D. Payan, H. Wulf, C. Imhof, D. Pitchford, and H. Zugaj, "Critical review of spacecraft charging standards," in *14th Spacecraft Charging Technology Conference*, 2016.

[49] D. Standard, "Spacecraft charging and discharging. japan aerospace exploration agency, safety and mission assurance department, 2012," tech. rep., Paper JERG-2-211A.

[50] M. Kruglanski, N. Messios, E. De Donder, E. Gamby, S. Calders, L. Hetey, and H. Evans, "Space environment information system (spenvis)," in *EGU General Assembly Conference Abstracts*, vol. 11, p. 7457, 2009.

[51] H. B. Garrett and A. R. Hoffman, "Comparison of spacecraft charging environments at the earth, jupiter, and saturn," *IEEE transactions on plasma science*, vol. 28, no. 6, pp. 2048–2057, 2000.

[52] N. Divine and H. Garrett, "Charged particle distributions in jupiter's magnetosphere," *Journal of Geophysical Research: Space Physics*, vol. 88, no. A9, pp. 6889–6903, 1983.

[53] V. M. Vasyliunas, "A survey of low-energy electrons in the evening sector of the magnetosphere with ogo 1 and ogo 3," *Journal of Geophysical Research*, vol. 73, no. 9, pp. 2839–2884, 1968.

[54] V. Pierrard and M. Lazar, "Kappa distributions: theory and applications in space plasmas," *Solar Physics*, vol. 267, no. 1, pp. 153–174, 2010.